Investigation into Pattern Synthesis and Target Tracking Techniques

University of Cape Town

Department of Electrical Engineering

2006

Supervised By:

Prof. M. Inggs

Prepared By:

Mr. G. Lange

Submitted in partial fulfillment of the requirements for the degree of Bachelor of Science in Electrical Engineering at the University of Cape Town

23 October 2006

Declaration

I declare that this undergraduate thesis is my own work. All sources I have used or quoted have been indicated and acknowledged in the references. This work has not been submitted for any degree or examination in any other university.

……………………… ………………………

Gunther Erich Lange Date

Acknowledgements

First and foremost I would like to thank Professor Mike Inggs for his extremely helpful and patient supervision. I would also like to thank my family and friends for their unwavering and continual support.

Abstract

The core objective of this thesis is to investigate various methods of target tracking and interference canceling within the field of passive radar. In particular, these methods were analysed by means of simulations within Matlab using half-wave dipoles as elements of a linear array.

This thesis begins with a brief background of a passive radar system noting the importance of beam forming and null placement within such a system. This is followed by a description of the main objectives and a detailed summary of each chapter of this report. Literature covering all aspects considered important and applicable to the topic of this thesis will be reviewed in detail.

The work done in this thesis is introduced in a modular fashion, beginning with the description of a single half-wave dipole element. Thereafter, a second element is added, forming an array. By means of simulations, ways of forming a beam in a particular direction and fixing a null in another direction were investigated. In addition, phase monopulse angle sensing techniques [4] were introduced and applied to the two element array in order to investigate methods of target tracking.

Next, a third antenna element was added to the array. In this arrangement, methods of independent null steering were considered. Furthermore, phase monopulse angle sensing techniques [4] in the presence of a target and an additional inference signal were reinvestigated and discussed, also using the three element arrangement.

Finally, conclusions were drawn for the core findings of this thesis and areas of possible future work were considered.

Table of Contents

List of Figures

List of Tables

List of Symbols

Symbol – Definition

$\hat{E}_{\theta}$ - Electric field in the direction of the spherical unit vector $\hat{\theta}$

I_0 - Magnitude of current at the feed of the antenna

r - Radial distance to point of interest

λ - Wavelength (c/f)

k - Wave number ($2\pi/\lambda$)

θ - Angle of elevation measured from the positive z axis

R - Distance to far-field

ϕ - Angle of azimuth measured from the positive x axis

s_1 - Distance between elements A and B

s_2 - Distance between elements B and C

$\hat{E}(\phi)$ - Electric field at a point in the azimuth

β - Additional phase delay

C - Gain

A - Half-wave antenna element A

B - Half-wave antenna element B

C - Half-wave antenna element C

$\hat{E}_1$ - Electric field at element A

$\hat{E}_2$ - Electric field at element B

$\hat{E}_3$ - Electric field at element C

γ - Angle to the target of interest from the reference axis y

γ_p - Angular range over which a target's angle can be accurately approximated

V_0 - A constant within the angle sensing circuit [4]

δ - Phase delay due to spacing

δ_1 - Phase delay of an incoming target signal in elements A and B

δ_2 - Phase delay of an incoming interference signal in elements A and B

δ_3 - Phase delay of an incoming target signal in element C

δ_4 — Phase delay of an incoming interference signal in element C

R_r — Radiation resistance

R_L — Loss resistance

P_r — Radiated Power

$\hat{E}_{element\ A}$ — The total electric field at element A

$\hat{E}_{element\ B}$ — The total electric field at element B

$\hat{E}_{element\ C}$ — The total electric field at element C

$\hat{E}_{sum}$ — Output response of the summation of all signals in the array

$\hat{E}_{TotInt}$ — Summation of all the interfering signals in all elements (Ch. 6)

q_0 — Real output response of a monopulse system

q_1 — Linear approximation of real output response for the proportional region

ϕ_{Int} — Angle to point of interference taken from the positive x axis

$\hat{E}_{1\ CLEAN}$ — Signal after the summation in channel 1 (Ch.7)

$\hat{E}_{2\ CLEAN}$ — Signal after the summation in channel 2 (Ch.7)

$\hat{E}_{xTar}$ — Electric field induced at element x by the target

$\hat{E}_{xInt}$ — Electric field induced at element x by the interference point

$\hat{E}_{C1\ INT}$ — Total interference component in channel 1 (Ch 7)

$\hat{E}_{C2\ INT}$ — Total interference component in channel 2 (Ch 7)

H — Gain (leads to channel 1)

G — Gain (leads to channel 2)

ε — Phase delay (leads to channel 1)

σ — Phase delay (leads to channel 2)

Glossary

GUI — Graphical User Interface

ARRL — American Radio Relay League

Chapter 1

Introduction

1.1   Background

The field of passive radar, in particular its application in the detection and tracking of targets, is currently enjoying much renewed interest. With today's ever-present ambient radio waves, such as television signals, the use of passive radar has been found to have some distinct advantages over the use of some other conventional radar systems [6].

An important factor for the effective use of passive radar systems is the ability of the system to form a beam in a particular direction so as to track a moving target while simultaneously forming a null in another direction to cancel out an undesirable interference. Interference may come from a variety of sources, but the interference received directly from the transmitter, whose reflected signal is used for target tracking, is of greatest concern. This emphasizes the importance of null formation.

The properties of nulls and beams are best described by analysing radiation patterns set up by an array of half-wave dipole antenna elements. The shape of a radiation pattern is determined by a variety of parameters specific to the array. By investigating these parameters and the subsequent radiation patterns simultaneously, much information can be obtained about the properties of the nulls and beams. In particular, relationships between different parameters can be noted.

1.2   Objectives

The objectives of this thesis are:

- To research literature related to the topic to form a sound foundation.
- To simulate an array of antenna elements.

- To enable the array to form a beam in a particular direction.
- To enable the array to form a null in a particular direction.
- To track the position of a target.

These objectives are in essence quite broad, allowing for a variety of methods and techniques to be investigated and used. Yet, due to the broad nature of the objectives the methods of the investigations and analyses in each chapter will be clearly stated.

1.3   Plan of Development

Chapter 1 forms the introduction to this thesis. The background to the topic is discussed and objectives of the project are presented here.

Chapter 2 is the literary review and presents various factors and information necessary and related to the thesis topic. The following topics will form the core to the literary review: The establishment of necessary antenna fundamentals, focusing in particular on the properties of a half-wave dipole. This will be followed by a description of the properties of a multielement array. Within this description beam forming and null placement techniques will be briefly reviewed. A method of antenna and electromagnetic wave modeling with Matlab presented by S. N. Makarov [5] will be discussed. These techniques were used extensively to understand the effects of spacing and phasing in antenna array design. Different types of monopulse sensing techniques for the purpose of angle measurement will also be reviewed in this chapter. As the antenna systems developed in this thesis form possible subsystems of a passive radar receiver some background to passive radar systems will be presented. In general, a brief history, advantages and disadvantages of the passive radar will be investigated. Finally, as television signals are generally used in passive radar applications some important properties of television signals are investigated.

Beginning with an investigation of a single half-wave dipole element the work done from here on in this thesis will proceed in a modular fashion, each chapter building on the last. Furthermore, each chapter ends with a conclusion of the findings of that chapter. This thesis is in essence an analytical thesis where different theory and

methods of antenna array analyses are investigated with the use of simulations in Matlab.

Chapter 3 will introduce a single half-wave dipole antenna element for investigation. This dipole element will form the core antenna element for the all following investigations. Its fundamental properties will be discussed and various simplifying assumptions will be stated. This chapter forms the foundation on which the other chapters will build. Matlab is used in this chapter to visualize some of the properties fundamental to a half-wave antenna element, such as its radiation pattern which clearly illustrates its omnidirectional nature.

Chapter 4 follows on from Chapter 3 with the addition of a second half-wave dipole element. The purpose of this chapter is to investigate different radiation patterns, to determine possibilities of simple beam synthesis and null placement. The radiation pattern of an array of two half-wave dipole elements can be manipulated by varying either the spacing between the elements and/or varying the phase feed in one of the two antenna elements with respect to the other. Matlab is used to analyse the relationship and effect of each variation on the radiation pattern. All investigations of radiation patterns will be limited to the azimuthal plane. The useful limits of element spacing as well as the useful limits of phase variation in the one element are determined here. The radiation patterns generated by the simulations are verified by a comparison with the radiation patterns published in the ARRL Antenna Handbook [1]. The two sets of patterns are found to be equal by inspection.

Ultimately, Chapter 4 shows that a variation of element spacing and phase delay (within the one element) gives rise to many different patterns. Some of these patterns are more favourable than others, presenting a more directive pattern, yet directivity is not exceptional in any case due to the simplicity of the array. Adding a reflector to the system could increase its directivity. Furthermore, it would be advantageous to form a null in the direction of a strong interfering transmitter. The two element array presented here, with variation of spacing and phase delay is not sufficient to steer nulls, though. This is because nulls move as a function of spacing and phasing. Thus, fixing of nulls in a particular direction cannot be achieved in a two element array when beam forming is necessary.

Chapter 5 focuses on monopulse phase sensing techniques for angle measurement. Using these techniques and the two element array described and discussed in Chapter 4, target tracking will be investigated. In particular, the multiplicative angle sensing ratio was used as a method to achieve angle measurement of a simulated target [4]. Assumptions were made to simplify the problem. One such simplifications as mentioned above, is the assumption that the target of interest only lies within the azimuthal plane at a constant radial distance. The target is also assumed to lie within the far-field of the antenna array and thus planar waves can be assumed. Yet another core assumption is that the magnitude of the electric field at each individual element is equal. All these assumptions and some others will be stated and reasons for them discussed. Matlab was used as the analysis tool whereby results were calculated.

The results showed the use of monopulse sensing techniques for angle measurement to be a successful method for tracking a target over a specified angular range (γ). Firstly, a favourable spacing range between the two antenna elements of $s_1 = 0.4\lambda$ to 0.95λ was found by investigating the effects of factors such as gradient response, ambiguity, feedpoint impedance and mutual impedance due to a change of spacing. Secondly, given this range and a further finding that a smaller element spacing would provide a greater angular range for tracking of a target, an element spacing of 0.5λ was chosen. 0.5λ was chosen over 0.4λ as it's pattern is well known and understood. An element spacing of 0.5λ will be regarded as the optimum element spacing for the optimum monopulse system, which will find further applications in later chapters.

The purpose of this **Chapter 6** is to investigate ways of steering a null in a particular direction with the aid of a third antenna element. The chapter will begin with a description of the antenna and receiver system arrangement. Various important properties of the three element array will also be stated and the electric field relationship between all points of interest will then be discussed. The formation of nulls due to a variation of spacing between the second and third element will be compared with the formation of nulls due to an added phase delay of the third element. Thereafter, a means to determine parameters that may accomplish cancellation of an interference signal received from any particular direction will be investigated.

In this chapter it was found that large values of spacing between the second and third element would be very unfavourable due to a rapid increase of sidelobes. Futhermore, the increase of sidelobes decreases the beamwidth of the major lobe, which is also undesirable in terms of target tracking. The radiation pattern produced by varying the phase delay of the third element while keeping the spacing constant did not show the serious degradation effects that an increase of spacing did. For this reason a variation of phase delay will be preferred over a variation of spacing when attempting null formation. In addition, there is a practical advantage of relying solely on phase variation, namely one would not need to physically move any antenna hardware as a variation of phase can be done electronically. Furthermore, from here on null formation will be investigated by varying only the phase and gain of the third element.

Chapter 7 investigates ways in which monopulse angle sensing can be achieved with the presence of an interfering signal. The third element, introduced in Chapter 6, will be used to attempt a cancellation of the interference within the first and second antenna elements by means of changing the phase delay and gain of the incoming signal in the third element. The chapter will begin with a description of the receiving system used. Monopulse angle sensing techniques will then be applied to the first two elements as was done in Chapter 5, starting with a situation where no attempt to cancel the interference is made. Thereafter, partial interference canceling will be dealt with and then finally full interference canceling will be investigated. Matlab was used as a tool whereby results were computed.

It was found in this chapter that if the interference is not canceled in the first two elements no phase monopulse sensing can be done. The method of partial interference canceling presented in this chapter proved successful, but required a variation of a number of parameters for accurate tracking of a target. This is not entirely favourable, as such a system would require significant signal analysis and control systems. The condition of full interference cancellation where the third antenna element is assumed directive was found to be very successful in terms of angle measurement. This method is the most desirable method when angle measurements are to be taken using phase monopulse techniques.

Chapter 2

Literature Review

The following review of literature was done on subjects that relate to or affect the subject of the project undertaken. Antenna fundamentals essential to the topic of the project will be discussed. Television frequencies will be investigated and a suitable frequency for the system will be chosen. A brief history and background of the passive radar system will be given. These discussions will form the basis and necessary background to work completed in this thesis.

2.1 Investigation of Antenna Fundamentals

Various properties of antennas will be discussed that are believed to be important.

2.1.1 The Principle of Reciprocity

During transmission a radar antenna functions as a transducer, converting the electrical waveform from the transmitter to an electromagnetic wave for transmission. On reception, the antenna performs the inverse function; it converts the arriving electromagnetic wave into an electrical waveform. It results that an antenna is a reciprocal device, which means that its behaviour during wave reception is known if its behaviour as a transmitting device is known. This fact allows us to study antennas principally as a radiating device [4].

In particular, the principle of reciprocity can be used when measuring antenna radiation patterns as its pattern while receiving is the same as that while transmitting [1, pg 2-13]. This fact is central to this thesis as radiation patterns will be investigated in detail.

2.1.2 Properties of an Elementary Radiating Element

Regardless of the system's application, all antennas have certain basic properties which can be well defined. The characteristics which are of most interest are the radiation pattern, polarization, gain and impedance [8, pg 8.1].

Radiation Pattern

The Radiation pattern of an antenna is generally the most basic requirement since it determines the spatial distribution of the radiated energy [8, pg 8.1]. The radiation pattern of an antenna in free space would be found by measuring the field strength at every point on the surface of an imaginary sphere having the antenna at its center [1, pg 2-13]. For analysis purposes, we consider the antenna to be located at the origin of a spherical coordinate system as shown below.
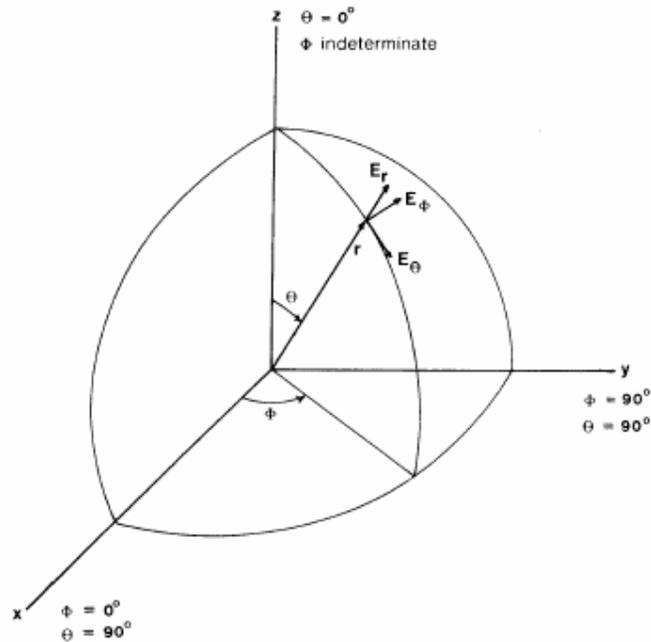
Figure 2.1: Spherical coordinate system used with antennas [9]

The pattern can be plotted versus either the angle θ (for the elevation plane pattern) or the angle ϕ (for an azimuthal plane pattern) [2, pg 115] and is usually plotted in two dimensions using polar or cartesian (rectangular) coordinates [9, pg 15]. The relative amplitude of the radiated energy may be recorded as a relative power pattern, a relative field pattern or a logarithmic decibel pattern [9, pg 15]. The relative field pattern shows the variation of electric field intensity at a fixed distance from the antenna as a function of angular coordinates described above [9, pg 16]. The logarithmic decibel relative gain pattern is given by $20\log_{10}(relative\ field)$ [9,pg 16]. The relative field pattern and the logarithmic decibel pattern will be central in analysis of radiation patterns in this thesis.

The most common radiating element is the electric current element, which is realized by a very short thin dipole or doublet. The exact radiation pattern of a linear antenna can be computed if the exact current distribution on the doublet is known [9, pg 50]. This is because the field radiated from such a linear element is proportional to the sum of elementary currents flowing in each part of the antenna element [1, pg 8-8].

After some simplifying assumptions the electric field pattern can be obtained by using the equation [9],

$$E_\theta = j60I_0 \frac{e^{-jkr}}{r} \frac{\cos((\pi/2)\cos\theta)}{\sin\theta} \quad V\!\!\Big/\!_m \qquad (2.1)$$

Where:

E_θ is the electric field in the direction of the spherical unit vector $\hat{\theta}$.

I_0 is the current magnitude at the feed of the antenna element.

k is the wavenumber given by $2\pi/\lambda$.

r is the radial distance to the observation point.

θ is the angle of elevation as described in Fig. 2.1

One condition for correct use of Eq. 2.1 is that the antenna element must be a half-wave dipole. Another necessary assumption is that the point of interest lies within the far-field region of the antenna element [9]. The far-field region of an antenna is given by

$$R = \frac{2L^2}{\lambda} \quad m \qquad (2.2)$$

where R is the far-field distance, L is the largest linear dimension of the receiving or transmitting antenna and λ is the wavelength [8, pg 8.3]. For electrically small antennas, this result may give a far-field distance that is too small; in this case, a minimum value of $R = 2\lambda$ should be used [2, pg 114].

Polarisation

The polarisation of an antenna is usually defined in terms of the orientation of the electric field vector in the direction of maximum radiation. In simple terms a vertical dipole will radiate vertically polarized signals [8, pg 8.1] and reciprocally the dipole antenna is capable of receiving those signals whose electric field has a component parallel to the dipole axis [5, pg 27].

The eTV and SABC television signals which are transmitted from the Tygerberg transmitter and which may be used in passive radar applications, are all vertically polarized [12].

Gain

Gain is closely associated with directivity, which in turn is dependent upon the radiation patterns of an antenna [8, pg 8.1]. We define antenna gain as the product of directivity and efficiency, to account for losses in the antenna [2, pg 118]. This implies that directivity of an antenna does not include the dissipative losses and is defined generally, in a specified direction (θ, ϕ) as [9, pg 21]

$$D(\theta,\phi) = \frac{4\pi \; power \; radiated \; per \; unit \; solid \; angle \; in \; the \; direciton \; \theta, \phi}{total \; power \; radiated \; by \; the \; antenna} \; . \; (2.3)$$

Both directivity and gain are expressed in dB as $D(dB) = 10\log(D)$ or $G(dB) = 10\log(G)$ respectively. Directivity (and subsequently gain) is often stated as relative to the directivity of an isotropic radiator, and written as dBi [2, pg 116].

Impedance [9 pg 29-30]

The self impedance is the impedance which would be measured at the input terminals of an antenna in free space. It is comprised of two components as follows: self impedance = (antenna resistance) + j(self reactance). The self reactance arises from the reactive energy stored in the near field. The antenna resistance is further comprised of radiation resistance and R_r and loss resistance R_L. The radiation resistance is defined as the equivalent resistance which would

dissipate a power equal to that radiated, P_r, when carrying the current flowing at the input terminals I_0, i.e.

$$R_r = \frac{P_r}{I_0^2} \, .$$

(2.4)

For a practical thin half-wave dipole for example, the radiation resistance may have a value approximately 73 Ω, with a loss resistance of perhaps 2 Ω.

2.2   Investigation of a Multielement Antenna Array

The gain and directivity offered by an array of elements represents a worthwhile improvement both in transmitting and receiving. One common method of obtaining gain and directivity is to combine the radiation from a group of half-wave dipoles [1].

2.2.1   *Important Properties and Fundamentals*

Each antenna element of an array can be referred to as a discrete source. The discrete sources radiate individually, but the pattern of the array is also determined by the relative amplitude and phase of the excitation fields on each source and the geometric spacing of sources [9]. In particular it is the constructive and destructive interference effects among the signals by the individual antenna elements (or discrete sources) that determine the effective radiation pattern of the array [12].

There are various types of multielement arrays and many different types of antenna element configuration for arrays. This thesis will deal solely with elements in a parallel configuration to form a linear array, where a linear array is an array in one dimension. An example is given below in Fig. 2.2.
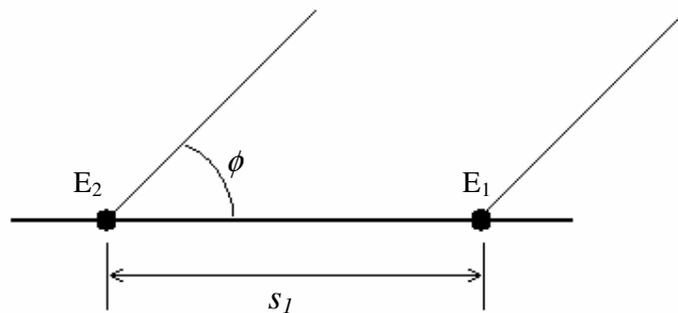
Figure 2.2: Two point source array [9]

10

The general expression for the far-field in the plane of the array is [9]:

$$\hat{E}(\phi) = \hat{E}_1 + \hat{E}_2 e^{-j(\beta + ks_1 \cos\phi)}$$ (2.4)

Where,

$\hat{E}_1$ is the electric field radiated by element A

$\hat{E}_2$ is the electric field radiated by element B

β is the additional phase shift in element B

s_1 is the spacing between the two elements

ϕ is the angle in the azimuth taken counterclockwise

The elements at A and B are treated as omnidirectional. The case of most interest is when the amplitude of the individual elements is equal, $\hat{E}_1 = \hat{E}_2$. In this case the radiation pattern is determined by the element spacing and the phase differential [9].

Consequently, many different shapes of patterns can be derived. In this case it is important to be able to classify different features of the patterns. For instance, the lobe having the maximum value is called the main beam, while those lobes at lower levels are called sidelobes [2].

A measure of the focusing effect is the 3 dB beamwidth of the antenna, defined as the angular width of the main beam at which the power level has dropped 3 dB from its maximum value (its half-power points) [2].

Mutual Impedance

Mutual coupling exists between any two conductors that are located near one another. Mutual coupling results in mutual impedance between two elements [1]. The mutual impedance has both resistive and reactive components. The actual input impedance of an antenna element is the sum of its self impedance and its mutual impedances with all other antennas in the vicinity such that,

Input Impedance = Self Impedance + Mutual Impedance [9].

The self impedance in the expression above is the impedance of an antenna element in free space and is defined in section 2.1.2 above.

The mutual coupling between antennas is important because it can have a significant effect (favourable or unfavourable) on the amount of power supplied. And it is the amount of current flowing in the antenna element that determines the field strength from the antenna. [1]

Granted that the mutual impedance is an important factor to consider, it will be disregarded for much of this thesis. It will however be used as a determining factor in Chapter 5.

2.2.2   *Beam-forming* [5]

There are certain advantages of beam-steering over a rotating radar antenna. A system that orients the antenna beam without the inertial effects of rotation allows all the possibilities of radar to be used in the full. It is in this way that the beam of a surveillance radar, scanning the horizon, can pause for an instant to confirm or disprove a possible alert. Similarly a tracking radar with electronic scanning can follow several targets by pointing at each of them successfully without any loss of time.

2.2.3   *Null Placement* [9]

Not only can we define wanted directions for receiving signals, we can also define the unwanted directions and achieve the latter by null steering (Placement). Null steering is desirable because some directions may contain high level interfering signals which must be minimized by means of these nulls. In particular, radar systems are susceptible to degradation in performance because of interference received through their sidelobes.

2.3 Monopulse Sensing Angle Sensing

By current technology the most-used, effective, and attractive method for deriving information about the spatial angles of a target is called monopulse. The name derives from the fact that the method is theoretically capable of obtaining estimates of a target's angles by using only one (mono) pulse [4]. Here some background and necessary concepts to the analysis of angle determination through angle-sensing monopulse will be discussed.

2.3.1 *Types of Monopulse Sensing Techniques* [4]

In general, there are three types of monopulse techniques of interest. One is called amplitude-sensing monopulse which makes use of the magnitude of the antenna patterns. The phase characteristics of the patterns are approximately the same and relatively independent of target angles. More than one pattern is essential for this sensing technique. The second monopulse technique is known as phase sensing monopulse and makes use of different phase characteristics of the patterns where the amplitudes of each pattern are approximately equal. The third type of monopulse is not clearly defined, but is often referred to as hybrid monopulse as this sensing technique makes use of both amplitude and phase sensing techniques.

2.3.2 *Pattern Representation*

The pattern presented by each element in an array can be described as an arbitrary one-way complex receiving voltage pattern by the notation $p(\theta_x)$ and the definition [4]:

$$p(\theta_x) = f(\theta_x)e^{j\beta(\theta_x)} \tag{2.5}$$

Where $f(\theta_x)$ is the amplitude of the pattern and $\beta(\theta_x)$ is its phase. Eq. 2.5 is a simplification for measurements in one coordinate [4]. For the investigations in this thesis, this simplified one coordinate expression will be adopted. Though, one further modification to this equation will be made as follows:

$$\gamma = \theta_x$$

$$\therefore p(\gamma) = f(\gamma)e^{j\beta(\gamma)} \tag{2.6}$$

The following modification was made so as to drop the unnecessary subscript x and will also simplify the notation in the monopulse analysis of angles in the Chapter 5.

2.3.3   Angle Sensing Ratios

Angle information can be obtained from investigating the ratio of a pair of patterns. Using a method whereby the ratios are investigated ensures that the angle measurement remains independent of target amplitude [4]. Two angle sensing ratios are dealt with by Peebles [4], namely the multiplicative and the additive angle-sensing ratios. The multiplicative angle-sensing ratio will be the one used in all investigation and analysis to follow, and is defined as:

$$r_m(\theta_x) = \frac{p(\theta_x)}{p(-\theta_x)} \tag{2.7}$$

And with the modification discussed in the section above the following is used:

$$r_m(\gamma) = \frac{p(\gamma)}{p(-\gamma)} \tag{2.8}$$

This forms the basic and necessary background to angle sensing monopulse.

2.4   Modeling of Antennas and Electromagnetic Waves

Methods of modeling antenna hardware and electromagnetic waves in Matlab, presented by Sergey N. Makarov [5], were extensively investigated and provided a useful introduction to how radiation patterns are affected by varying factors such as spacing and phasing.

2.4.1   Antenna Structures [5]

Matlab provides several ways of creating antenna structures. One way is to use the built-in mesh generator of the Matlab PDE toolbox. This mesh generator creates planar structures of any rectangles, polygons and circles. Another way is to identify the boundary of the antenna structure analytically. Then Delaunay triangulation is applied to that structure, using Matlab delaunay.
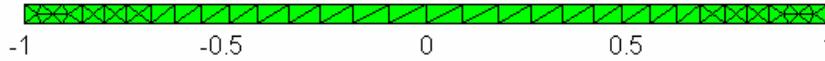
Figure 2.3: Half-wave antenna element using Matlab PDE Toolbox [5].

The figure above illustrates a half-wave dipole element. The triangles forming a mesh structure within this element can be clearly seen. This element is either fed or the receiving signal is measured at the point indicated by 0. The dimension values of this particular element are not important. Yet, in terms of dimensions an important thing to note is that this model is a strip, i.e. it has no dimension of depth (into the page). Be this as it may, the radius of the equivalent cylindrical wire is given by [5]:

$$a_{eqv} = 0.25s$$

Where s is the strip width, found in the figure above along the x-axis.

2.4.2 Method of Analysis

The analysis procedure (method of moments) used in this text relies on RWG (Rao-Wilton-Glisson) edge elements [5]. The surface under study is divided into separate triangles as shown and a basis function is assigned to the edge elements which are common edges between any two triangles. The division of the antenna structure into RWG edge elements approximately corresponds to the division of the antenna current into small "elementary" electric dipoles [5, pg 1-6]. Using RWG edge elements for modeling antennas obtained encouraging results. Faithful reproductions of the surface current distribution, input impedance, and gain are observed for dipole and monopole antennas [5].

The core of the book consists of two relatively short scripts: The first script computes the impedance matrix Z. The impedance matrix allows one to determine electric currents flowing through the antenna surface. The second computes the radiated field of an infinitesimally small electric dipole or a group of dipoles at any point in space. This code[1] helps one to determine near and far-field of an antenna, including its radiation patterns and gain [5].

---

[1] See Appendix D for the Makarov Code Sequence diagram

To investigate custom antenna structures the mesh input must be changed. The robustness of these code segements is such that the code sequence can be applied to many different arrays.

2.4.3 Antenna Arrays

The methods and code provided by Makarov [5] enables one to investigate various structures of antenna arrays. Antenna arrays can be produced by cloning single antenna elements, such as the half-wave dipole illustrated in Fig. 2.3 above. The text that was dealt with gave a thorough investigation into linear arrays of dipoles, focusing in particular on end-fire and broadside radiation behaviour.

Antenna arrays can be designed to control their radiation characteristics by properly selecting the phase/amplitude distribution and spacing between the elements. Also, the input impedance of a single antenna in an array will be different from that in free space, due to mutual coupling between antenna elements [5]. This is an effect taken into account by Makarov's code sequence.

2.5 The Passive Radar System

This thesis researches antenna properties relevant to passive radars. Passive radar systems require that the antenna subsystems cancel out unwanted direct signals in the echo channels to prevent masking of small echo signals [6]. To this end beam synthesis and null steering techniques are important features to a passive radar. For instance, a null would need to be fixed in the direction of the strong transmitter canceling out the direct signal. Also, to track small echo signals monopulse tracking techniques and beam synthesis are important and subsequently also discussed in this thesis. To give a better understanding of the passive radar system some background was investigated.

2.5.1 Structure of a Passive Radar System

In general, the transmit and receiving stations can exist at the same location or can have separate locations [4 ch1]. In the latter case the system is known as either bistatic or multistatic. In the monostatic system, which is more typical, a single

antenna often performs both transmit and receive duty [4]. This having been said, it must be noted that the word passive, in the expression passive radar, implies that the system does not have its own transmitter. A passive (bistatic or multistatic) radar usually makes use of ambient signals from transmitters such as Television Broadcasts, FM radio, cellular, enemy radar systems and space platforms (communication and navigation satellites) [6]. A passive bistatic radar system would comprise of one receiver and a one transmitter separated by substantial distance, where the transmitter would be a third-party transmitter as described above. A passive multistatic radar system would comprise of a one transmitter and more than one receiver, again where the transmitter is a third-party transmitter all separated by substantial distances [6]. In essence, the antenna structures developed and discussed in this thesis form smaller subsystems (or receiver modules) to a particular passive radar system. This project will investigate the core properties of one such subsystem or receiver module.

2.5.2   Brief History

Various early forms of radar devices were developed between about 1903 and 1925 that were able to measure distance to a target (the range) besides the targets presence [4, ch1]. These early radars were all essentially bistatic because the technology to enable an antenna to be switched from transmit to receive mode had not been developed [6].

Bistatic radar systems gave way to monostatic systems with the development of the synchronizer in 1936. The monostatic systems were easier to implement since they eliminated the geometric complexities introduced by the separate transmitter and receiver sites. In addition, aircraft and shipbourne applications became possible as smaller components were developed [6].

In the early 1950s, the bistatic (and multistatic) systems were considered again when some interesting properties of the scattered radar energy were discovered [6]. Research on passive radar systems is of growing interest throughout the world, with various open source publications showing active research and development [6].

2.5.3 *Advantages and Disadvantages of Passive Radar*

Some advantages and disadvantages of passive radars are shown below.

The advantages are [6] [7]:

- Cheaper purchase and operations & maintenance costs.
- Covert operation of receiver(s).
- Detect targets continuously, typically once a second.
- May detect some types of stealth aircraft better than conventional radar systems.
- Non-intrusive – No frequency allocation – allowing deployment in areas where normal radars cannot be deployed.
- Physically small and hence easily deployed.

The disadvantages are [6] [7]:

- A reliance on third-party transmitters, giving the operator little control over the availability of the illuminator.
- Line of sight is required between the transmitter and target, the target and the receiver and also the receiver and the transmitter (or a network connection).

2.6 Investigation of Television Signals

Television signals transmitted from the Tygerberg transmitter are intended to be the type of signal used for the application a hypothetical passive radar system and thus their nature and form will be investigated.

2.6.1 *International Frequency Allocation*

Broadcasting frequency bands are pre-planned and internationally coordinated through the ITU to avoid mutually harmful interference between neighbouring countries. The current international UHF television frequency assignment for South Africa, as set out by the ITU in the Geneva plan of 1989 is 470 MHz to 854 MHz. The allocation agrees with UHF Band IV and UHF Band V to ITU Region 1 which includes South Africa and most of its surrounding states [10].

2.6.2 *Analysis of the Television Signal*

The UHF television broadcasting band between 470 MHz and 854 MHz contains 48 channels, each of 8 MHz bandwidth [10]. The vision carrier is located 1.25 MHz above the lower edge of the 8 MHz band [10]. So for instance, channel 46 the vision carrier would be located at 671.25 MHz.

2.6.3 *Application to Thesis*

Channel 46 will form the band of interest in all the investigations done in this thesis project. In particular, though the vision carrier at 671.25 MHz is of most interest, 674 MHz will be treated as the center frequency and will also be assumed to be the operating frequency for all antenna systems.

Chapter 3

Single Half-Wave Dipole Element

The purpose of this chapter is to introduce the half-wave dipole antenna element. This chapter will in particular investigate the important properties of the half-wave dipole discussed in the literature review such as the radiation pattern and polarization. The investigation of this antenna element is important because it forms the fundamental antenna element of the following chapters which deal with multiple antenna elements. The analysis of these properties will be performed by a script written in Matlab.

3.1   Basic Properties and Fundamentals

The structure of the half-wave dipole is given below:
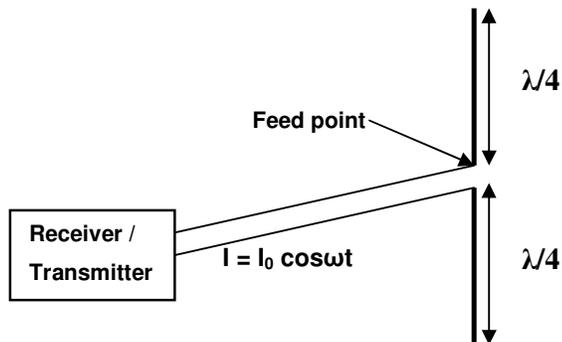
Figure 3.1: Structure of a half-wave dipole element

Fig. 3.1 illustrates the basic dimensions of a single half-wave antenna element which consists of two quarter-wave ($\lambda/4$) elements. It also shows how this antenna would be simply connected to a transmitter or receiver through a pair of parallel wires with a feed into the center of dipole antenna [11]. For the following analysis this antenna will be considered located at the origin of the spherical coordinate system described in Chapter 2 with the axis of the dipole along the z axis of the coordinate system. A dipole orientated in such a way is known to be vertically polarized, which means that the electric field generated by this antenna will also be vertical.

Investigations on all following antenna structures will be done at a center frequency at 674 Mhz as discussed in the literature review. The specification of this frequency will determine the resonant length of the half-wave dipole.

3.2   The Electric Field and Radiation Pattern

Half-wave dipoles are simple antenna elements and have been studied for many years. This fact allows us to use some well known equations to calculate and approximate the electric field at certain points around the antenna. In particular, their radiation patterns can be plotted and thus physically visualized with the use of the following well known equation given in chapter 2 describing the electric field vector [9]:

$$\hat{E}_\theta = j60I_0 \frac{e^{-jkr}}{r} \frac{\cos((\pi/2)\cos\theta)}{\sin\theta} \quad V/m \qquad (3.1)$$

At this point a simplifying assumption is made such that the angle of elevation θ, is set to 90° which means that our investigation is confined to the azimuthal plane. Throughout this investigation, the electric fields within the elevation plane will not be considered.

Furthermore, for the following investigation the radial distance r will be assumed constant around the antenna element. In addition, for this equation to hold, the radial distance must ensure that calculations are done in the far-field, i.e. r >> R. Where R is the radial distance to far-field region. Using the equation $R = 2L^2/\lambda$ defined in Chapter 2, gives a result too small. Thus a conservative estimate of $R = 2\lambda$ [2] to determine far-field is used and finds R = 0.89 m (for the center frequency 674 MHz). This implies that our investigation must choose r >> 1 m.

Taking these simplifying assumptions into account, Eq. (3.1) reduces to:

$$\hat{E}_\theta = j60I_0 \frac{e^{-jkr}}{r} V/m \qquad (3.2)$$

This equation will produce an electric field vector with a constant magnitude at a constant radial distance.

3.3 Computation of Radiation Pattern

The Matlab script SingleElement.m[2] uses the aforementioned theory to calculate the electric field at a constant radial distance around the antenna element. Subsequently, the radiation pattern due to the electric field is also generated. The necessary input variables required by the script and their current equivalent values are listed in Table 3.1.

Table 3.1: Necessary inputs to the SingleElement.m script.

Variable	Value
Radial Distance r (m)	1000
Current Amplitude I_0 (A)	1
Center Frequency f (MHz)	674
Speed of Light c (m/s)	299.79

The variable values can be changed for different investigations. As discussed the radial distance *r* has been chosen very large as to ensure far-field investigation. The center frequency 674 MHz has been discussed and the speed of light is simply a constant. The current amplitude was assumed to be 1A.

The code within the script is looped in such a way that the electric field is calculated using the variables of Table 3.1 at incremental angular positions in the azimuthal plane over the entire bearing range such that $\phi \in [0°, 360°]$. This procedure allows one to visualize the shape of the radiation pattern due to the electric field.

3.4 Results

Running the script SingleElement.m with variable values specified in Table 3.1 results in a vertically polarized electric field at the given radial distance:

$$\hat{E}_\theta = 0.059 + j0.011 \ V/m$$

---

[2] See Appendix E.1 for a detailed description of the Matlab script concerned with this chapter.

Furthermore, the electric field was found constant over the entire range of the azimuth angle $\phi \in [0°, 360°]$ at the given radial distance from the origin of the spherical coordinate system described in Chapter 2. The electric field found above is complex. Of greater interest is the magnitude which is calculated to be $|E_\theta| = 0.06$ V/m. Using the magnitude of the electric field the radiation pattern can be plotted in a polar coordinate system. For instance the resulting plot from this investigation is illustrated in Fig. 3.2 below.
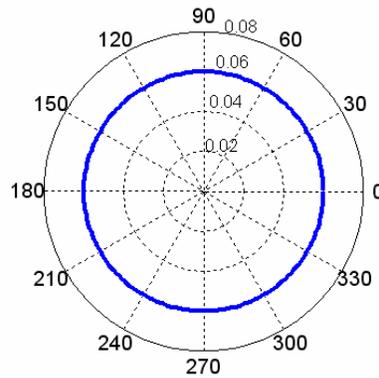
Figure 3.2: Amplitude radiation pattern of a single dipole element.

The figure above is a plot of the amplitude radiation pattern and clearly shows the magnitude of the electric field as constant for all angular positions in the azimuthal plane.

3.5   Conclusions

These results were as expected. Fig. 3.2 illustrates the classic omnidirectional nature of the half wave dipole antenna with constant electric field at a radial distance r from the antenna located at the origin of the coordinate system.

Chapter 4

Two Element Dipole Array

Chapter 4 follows on from Chapter 3 with the addition of a second half-wave dipole element. The purpose of this chapter is to investigate different radiation patterns and to determine possibilities of simple beam synthesis and null placement. The radiation pattern of an array of two half-wave dipole elements can be manipulated by varying either the spacing between the elements and/or varying the phase feed in one of the two elements. Matlab is used to analyse the relationship and effect of each variation on the radiation pattern. Our investigation of all radiation patterns will be limited to azimuthal plane. The useful limits of element spacing as well as the useful limits of phase variation in one of the elements are determined here.

4.1   Basic Properties and Fundamentals

The basic antenna arrangement of two, half-wave elements is illustrated below.
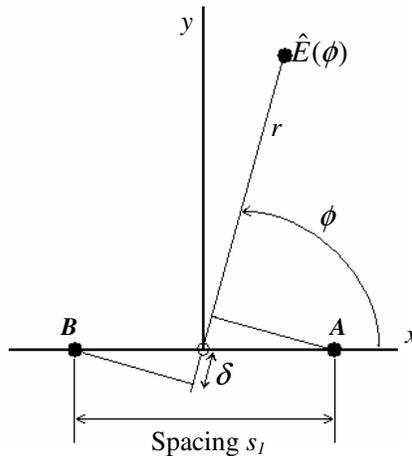
Figure 4.1: Arrangement of a two half-wave dipole array

Fig.4.1 shows the antenna elements located at the positions A and B. These elements are orientated parallel to the z axis and thus will be viewed as point sources here [9]. There will be electric fields $\hat{E}_1$ and $\hat{E}_2$ set up at points A and B respectively such that the electric field $\hat{E}(\phi)$ in the far-field region and at an angular position ϕ in the azimuth is given by [9,11]:

$$\hat{E}(\phi) = \hat{E}_1 e^{+j(\beta + k\frac{s_1}{2}\cos\phi)} + \hat{E}_2 e^{-j(k\frac{s_1}{2}\cos\phi)} \quad V/m \qquad (4.1)$$

In the equation above $k = 2\pi/\lambda$ (wavenumber), s_1 is the spacing between the elements in meters and $\hat{E}_1$ and $\hat{E}_2$ are both electric fields described by the Eq. 3.2 of the previous chapter. Note also that the phase center of this two element array is chosen at the origin of the coordinate system. This has the effect that fields $\hat{E}_1$ and $\hat{E}_2$ are either leading or lagging in phase relative to the position of $\hat{E}(\phi)$. This varying phase lead and lag is given by δ in Fig. 4.1 and is represented in Eq. 4.1 as the term $k(s_1/2)\cos\phi$ [9].

Lastly, note that an added phase delay can be introduced with β in the first term on the right hand side.

Some simplifying assumptions to the above deductions are made as follows. Firstly, $\hat{E}_1$ and $\hat{E}_2$ have equal amplitude. Secondly, the investigation is once again confined to the azimuth. Thirdly, planar waves can be assumed to arrive at antenna array as the point of interest $\hat{E}(\phi)$ lies in the far-field.

4.2 Computation and Analysis

Using the derivations above some Matlab scripts[3] were written. The diagram below illustrates the code sequence:
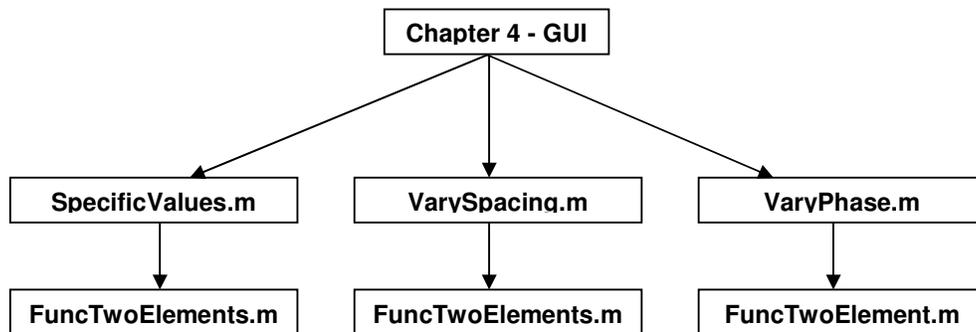
Figure 4.2: Code Flow Diagram

---

[3] See Appendix E.2 for a detailed description of the Matlab scripts relevant to this chapter.

The objective of this code was to generate radiation patterns for visualization and analysis purposes. The GUI (ch4_GUI.m) provides the user with three different analysis choices, which are achieved by the three scripts SpecificValues.m, VarySpacing.m and VaryPhase.m. These scripts are in essence plotting functions. They plot the logarithm of the voltage signal of Eq. 4.1 on a linear decibel grid [1]. The script FuncTwoElements.m is called by each of the three m.files above to calculate the electric field in the far-field region (using Eq 4.1), for a specific phase and spacing.

The script SpecificValues.m simply calls FuncTwoElements.m once and plots the radiation pattern. The input parameters to SpecificValues.m are specified in the GUI.

The script VarySpacing.m is a loop in essence, which calls FuncTwoElements.m as it loops incrementing spacing between the elements. This script requires a constant phase value to be set. Again, these input parameters can be set in the GUI. The output of VarySpacing.m is a surface plot of varying spacing, electric field and azimuth angle.

Finally, VaryPhase.m is similar to VarySpacing.m, the only difference being that the phase is incrementally looped while calling FuncTwoElements. This script requires a constant spacing parameter. Similarly, a surface plot is also generated. The use of a GUI aids in the quick generation of radiation patterns and enables input parameters to be changed easily.

4.3   Verification

To verify the code described above comparisons can be made with the radiation patterns published in the ARRL Antenna Handbook [1]. All the combinations of spacing and phasing to produce the patterns shown in Fig. C.1[4] were tested and found to be in close approximation to the radiation patterns generated by the code. This served as the necessary verification of the code to generate patterns. As an example two sets of plots will be compared.

---

[4] See Appendix C for the radiation patterns published in the ARRL Antenna Handbook

For the first comparison, a spacing = λ/2 and a phase delay = 0 rad is chosen. This is a well known combination which should illustrate a bidirectional broadside pattern. The plot generated by the GUI is illustrated in Fig. 4.3(a) and it's ARRL [1] equivalent is shown in Fig 4.3(b).

(a)   (b)
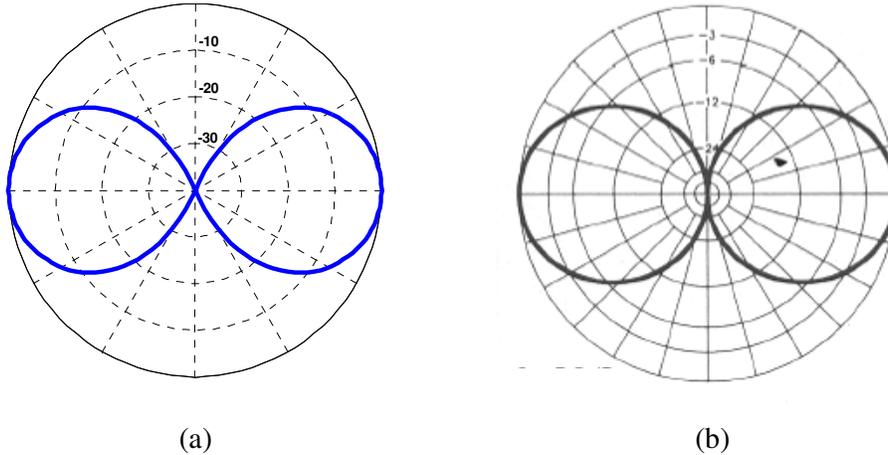
Figure 4.3: Radiation patterns (spacing = λ/2, phase = 0 rad) generated by (a) the simulation GUI and (b) the ARRL [1]. The azimuth angle ϕ starts at the vertical and proceeds counterclockwise.

Noting that the azimuth angle ϕ starts at the vertical and proceeds counterclockwise, refer to Fig. 4.1 to attain a sense of antenna arrangement. Both radiation patterns are obtained from the logarithm of the voltage in the signal [1]. A slight difference in these two plots is the log grid. Fig 4.3(a) uses a linear decibel grid known as the standard log grid [1], where Fig 4.3(b) uses a log grid system of concentric grid lines spaced periodically [1]. In essence they depict the same relationship and thus by inspection the two radiation patterns are found equal.

For the second comparison, a spacing of 7/8λ and a phase delay of $\pi/2$ rad was chosen.

(a)   (b)
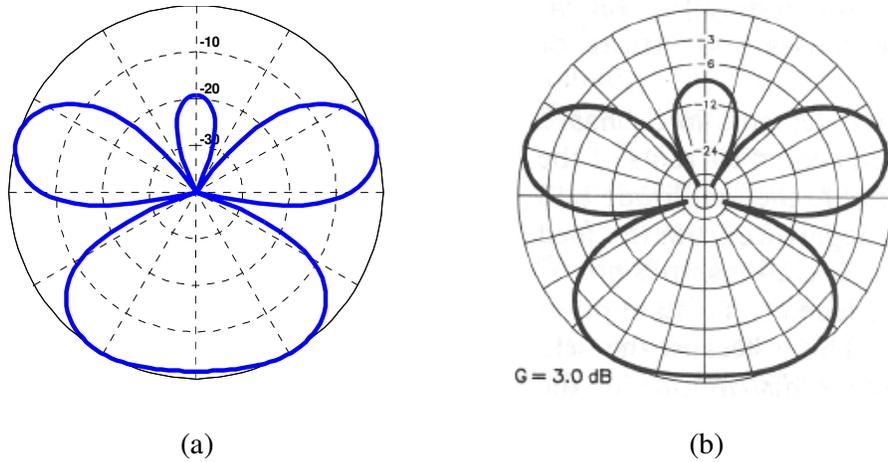
Figure 4.4: Radiation patterns (spacing = 7/8λ, phase $= \pi/2$ rad) generated by (a) the simulation GUI and (b) the ARRL [1]. The azimuth angle ϕ starts at the vertical and proceeds counterclockwise.

The same properties described for Fig. 4.3 are applicable to Fig 4.4 and subsequently by inspection the patterns are found to be roughly the same, thus providing the necessary verification of the code.

4.4 Observation of Radiation Patterns

By varying the spacing and the phase of the antenna elements, a virtually infinite amount of patterns can be generated [1]. However, effective variation of these two factors could achieve favourable directive patterns. The use of the surface generator (ch4_GUI.m) is useful in visualizing the change in radiation pattern due to a variation of one of these factors. Here, the surface generator will be used to make observations on the varying radiation pattern.

Firstly, if the phase delay β is kept constant at 0 rad and the spacing (s_1 in Eq. 4.1) is varied the following shape is generated by the surface generator, as illustrated in Fig.4.5.

28
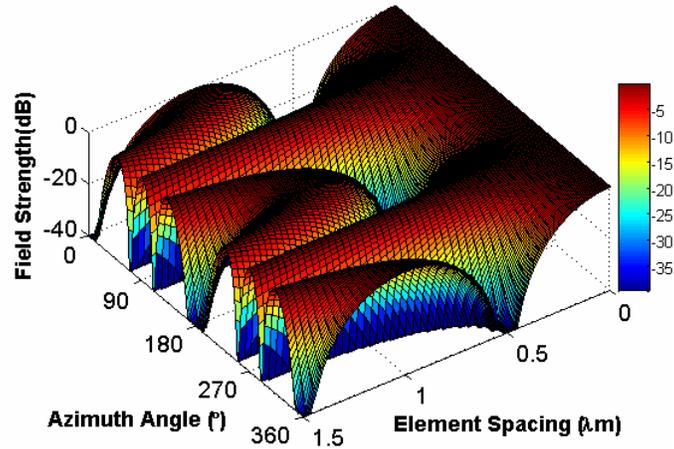
Figure 4.5: Surface of Radiation Pattern due to a varying spacing (0λ to 1.5λ) between elements.

Noting the colourbar the following observations are made. At a hypothetical zero spacing the pattern is virtually omnidirectional. As the spacing is increased to $\lambda/2$ the pattern becomes more directive in the directions of 90° and 270° and less so in the directions 0° (360°) and 180° in the azimuth. Subsequently, at $\lambda/2$ the pattern is said to be broadside, with nulls having formed in the directions of 0° and 180° with maximum response in the 90° and 270° directions. As the spacing is increased further to 1λ, sidelobes start to occur at the original position of the nulls at 0° and 180° in the azimuth. Above 1λ the pattern starts to repeat itself, with the formation of more sidelobes. This effect is undesirable, as the signal reception becomes ambiguous with degeneration of directivity. For this reason, spacing of an omnidirectional antenna array is usually kept below 1λ.

Now, varying the phase β in Eq. 4.1 with respect to a constant spacing, say $\lambda/2$, observations are made with reference to Fig. 4.6 below.
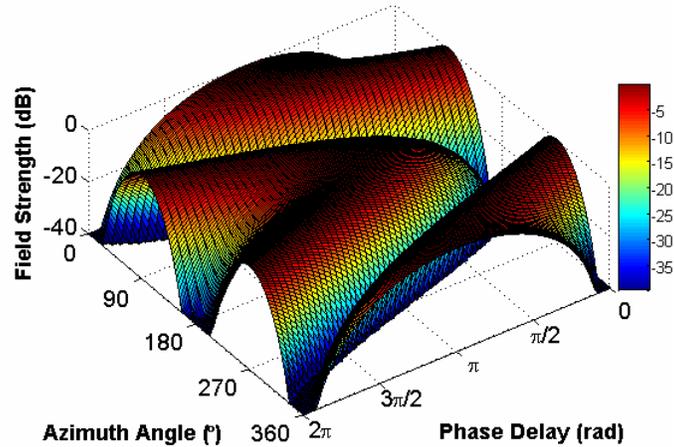
Figure 4.6: Surface of Radiation Pattern due to a varying phase (0 to 2π rad) between elements.

At $\beta = 0$ rad phase delay, the pattern generated is effectively broadside as described above. As the phase delay is increased to π rad the radiation pattern changes until its maximum response is in the azimuth directions 0° (360°) and 180° with nulls having been formed in the 90° and 270° azimuth directions. The pattern at this phase (π rad) is known as a bidirectional endfire pattern. Increasing the phase delay further to 2π rad sees a change of radiation pattern back to its original broadside pattern. An increase in β above 2π will see a repetition of variation just explained.

4.5   Discussion of Radiation Patterns

This type of variation of phase feed delay can achieve very simple forms of beamsteering. So, in order to obtain maximum response from a signal in particular direction it is favourable to orientate the beam (major lobe) formed by the antenna array, so that it points towards that signal. This is made possible by varying the element spacing and the added phase delay as shown above.

The radiation patterns were seen to be generally bidirectional. This could become a drawback as undesirable interference can be easily picked up from behind. Thus ambiguity may play a significant role when the direction of arrival is important to be known.

30

4.6   Conclusions

Varying the element spacing and phase delay (within one element) gives rise to many different patterns. Some of these patterns are more favourable than others, presenting a more directive radiation pattern, yet directivity is not exceptional in any case due to the simplicity of the array. Adding a reflector to the system could increase its directivity.

Furthermore, it would be advantageous to form a null in the direction of a strong interfering transmitter. The two element array presented here, with variation of spacing and phase delay is not sufficient to steer nulls, though. This is because nulls move as a function of spacing and phasing. Thus, fixing of nulls in a particular direction cannot be achieved in a two element array when beam forming is necessary.

Chapter 5

Angle Sensing using Phase Monopulse

This Chapter focuses on monopulse phase sensing techniques for angle measurement. Using these techniques and the two element array described and discussed in Chapter 4, target tracking will be investigated. In particular, the multiplicative angle sensing ratio was used as a method to achieve angle measurement of a simulated target [4]. Assumptions were made to simplify the problem. These assumptions will be stated and reasons for them discussed. Eventually the limitations of this monopulse angle measurement technique will be investigated and discussed. Matlab was used as the analysis tool whereby results were calculated.

5.1 Basic Properties and Antenna Arrangement

In general the same structural setup introduced in Chapter 4 will be used with some minor changes. The antenna arrangement is given below in Fig. 5.1.
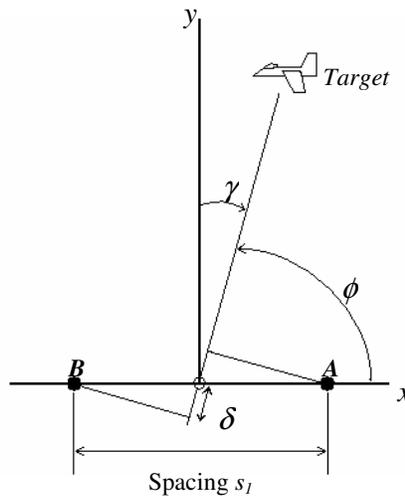

Figure 5.1: Antenna and sensing system arrangement

In this chapter the angle γ will be of major importance to the investigation. This angle γ will indicate the angle of the target of interest from the reference axis y shown in Fig 5.1. Otherwise, the same setup described in Chapter 4 will be used

32

where the spacing between the two elements is represented by the variable s_1. The azimuth angle is ϕ, and the phase center of the antenna system will be located at the origin. The half-wave antenna elements are represented by the letters A and B.

5.2   Simplifying Assumptions

Again it is assumed that the target of interest is confined to the azimuthal plane. Also, it will be assumed that this target follows a circular path around the phase center of the antenna array at a certain large and constant radial distance. In addition, the wave arriving at the antenna array is planar as the target will be assumed to be lying in the far-field region. Yet another core assumption is that the magnitude of the electric field at each individual element is equal.

5.3   Electric Field Relationships

Using the principle of reciprocity the following deductions were made. The electric field at the target is given by $\hat{E}(\phi)$. The electric fields at the antenna elements A and B are $\hat{E}_1$ and $\hat{E}_2$ respectively. As a recap the electric fields at A and B were set up using the Eq. (3.2).

It must also be reiterated that the amplitudes of $\hat{E}_1$ and $\hat{E}_2$ are equal. The relationship between the electric field at the target and the elements is given by:

$$\hat{E}(\phi) = \hat{E}_1 e^{j(k\frac{s_1}{2}\cos\phi)} + \hat{E}_2 e^{-j(k\frac{s_1}{2}\cos\phi)} \; V/m \qquad (5.1)$$

This is the same equation used in Chapter 4 if β is disregarded. Again, it can be seen how the principle of reciprocity is made use of, in the sense that we are interested in the electric fields received at elements A and B by the target, but in essence they have already been set up, producing the electric field at the targets position using Eq. 3.2 and 5.1.

A slight modification will be made to the above equation to aid analysis in of in terms of phase monopulse. The phase advance and delay (shown in Fig. 5.1 as δ) of the

respective elements A and B, receiving a signal from the target, are manipulated to give[5]:

$$|\delta| = k \frac{s_1}{2} \sin(\gamma) \qquad (5.2)$$

This modification was done in accordance with [4]. Subsequently (5.1) becomes:

$$\hat{E}(\gamma) = E_1 e^{j(k\frac{s_1}{2}\sin\gamma)} + E_2 e^{-j(k\frac{s_1}{2}\sin\gamma)} \; V/m . \qquad (5.3)$$

The necessary electric field properties have now been set up.

5.4   Computation and Analysis

The multiplicative angle sensing ratio [4] will be used to determine the relationship between spacing of elements and angle of arrival γ. The real output q_0 can be shown to be proportional to γ for small angles of γ [4] by the equation[6]:

$$q_0 = \frac{V_0^2}{2} \sin(\frac{2\pi s_1}{\lambda} \sin \gamma) . \qquad (5.4)$$

Implementing Eq. 5.4 in the Matlab script PhaseMonopulse.m, computes the response of q_0 relative to a variation of γ. The core input parameters listed in Table 3.1 are used with the addition of a couple others seen, in particular, in Eq. 5.4. V_0 is a constant representing certain amplitudes of signals within the sensing circuit [4] and will simply be assumed equal to 1. The spacing of elements is set at $s_1 = \lambda/2$ and the angle of arrival is investigated over the range $\gamma \in [-90°, \; 90°]$.

Subsequently, the relationship between q_0 and γ is illustrated in Fig 5.2 below.

---

[5] See Appendix A.1 for detailed derivation

[6] See Appendix A.2 for detailed derivation of multiplicative sensing ratio and output response q_0
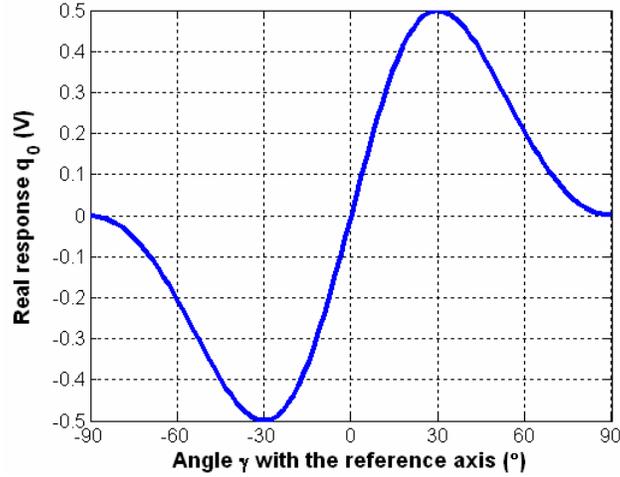
Figure 5.2: Relationship between the real output response q_0 and angle γ with the reference axis.

The real response can be seen to be sinusoidal, but also note that for small angles around $\gamma = 0°$ the response can be approximated proportional. A new variable γ_p is now specified and defined as the angular range over which the response q_0 can be approximated proportional. To find the angular range of γ_p, the following computation was done. Peebles's deduction for $|\gamma|$ small, where $K = -V_0^2 \pi \, s_1 / \lambda$ (a constant), is now used [4]:

$$q_1 \approx -K\gamma \qquad\qquad (5.5)$$

This relationship between q_1 and γ is plotted over the entire range of interest, $\gamma \in [-90°, \ 90°]$ and is presented in Fig. 5.3 as line A.
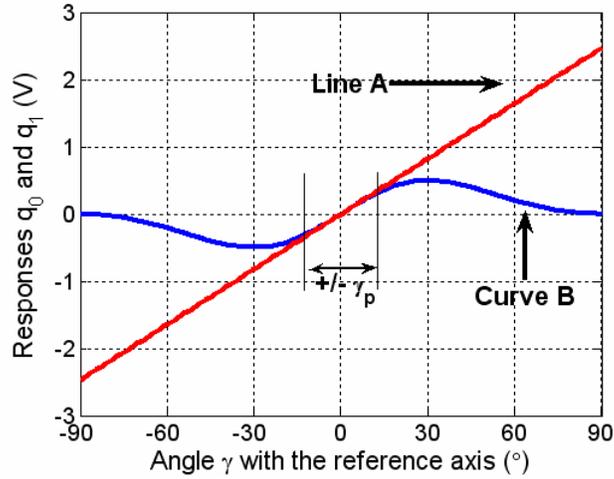
Figure 5.3: The response of q_0 (Curve B) and q_1 (Line A) as a function of γ.

The response illustrated in Fig. 5.2 is also shown in Fig. 5.3 as the curve B to give a visual comparison. Also seen in Fig. 5.3 is an approximation of the proportional region of curve B in terms of γ_p.

The region γ_p is of major interest, because the proportional behaviour would allow one to determine the angle of arrival by measuring a proportional output voltage from the sensing circuit. Also, it would be preferable for this region to be quite large. A large γ_p would enable tracking of targets over a greater range. Now, to find γ_p the following expression was implemented in the script PhaseMonopulse.m:

$$|q_1 - q_0| \leq error \tag{5.6}$$

This equation gives an approximation of the range of γ_p within a specified error. The error for the following calculation will be set at 0.05.

So, fixing the variable V_0 and λ of Eq. 5.4 and varying the spacing s_1 between elements A and B would result in a variation of the responses q_0 and q_1. Note figure 5.4 below.
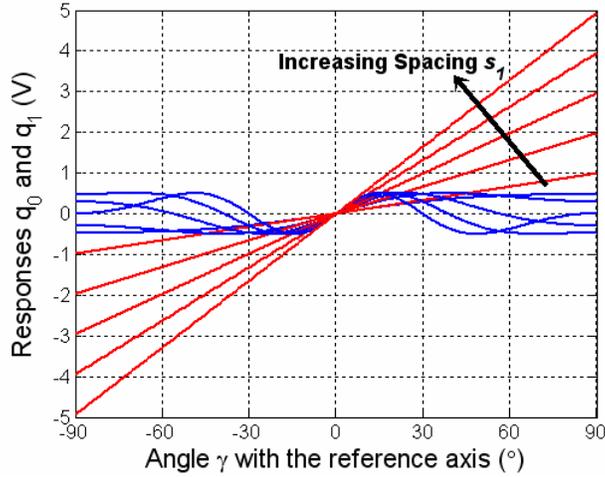
Figure 5.4: The response of q_0 (blue) and q_1 (red) as a function of γ with a varying spacing.

For an increase of spacing two things are noted in Fig. 5.4 above. Firstly, both the gradient of the response q_1 over the entire range $\gamma \in [-90°,\ 90°]$ and the gradient of the response q_0 for $|\gamma|$ small around the reference axis increase. Secondly, a decrease in angular range γ_p also occurs with an increase of spacing. The variation of γ_p due to a variation of spacing is not very clearly seen in Fig 5.4 but can be readily observed in Table 5.1. The angular ranges γ_p are calculated using the error equation Eq. 5.6.

Table 5.1: Variation of angular ranges with spacing

	Spacing s_1 (m)	Angular Range γ_p (°)
1	0.2λ	67.2
2	0.4λ	37.2
3	0.5λ	30.0
4	0.6λ	25.2
5	0.8λ	19.2
6	1λ	14.4

The objective was to find limiting factors to the monopulse sensing technique and to state the conditions for the optimum performance. Thus, Table 5.1 can be expanded to better visualize the relationship between the spacing between elements and the proportional range γ_p.

PhaseMonopulse.m was subsequently looped by the script LoopPhaseMonopulse.m to generate a relationship between γ_p and spacing s_1 between elements.
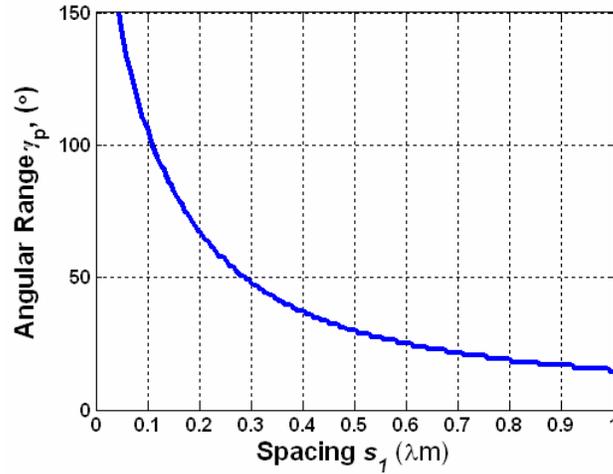
Figure 5.5: Relationship between spacing s_1 and angular acceptance range γ_p

Looking at the above figure one can see that the smaller the spacing, the greater the proportional range γ_p. Note the inverse relationship:

$$\gamma_p = k \frac{1}{s}$$

Where s is the spacing between elements and lowercase k is a proportionality constant.

5.5 Discussion of Results

To find the optimum spacing so as to achieve maximum feasible γ_p some important factors such as response gradient, ambiguity and input impedance must be taken into account. These will be discussed using the results from above.

5.5.1 Response Gradient

The core requirement is that of maximum proportionality range γ_p. For this reason, the spacing between elements would be preferred to be as small as possible. An extremely small spacing would not be feasible though, as the response gradient becomes immeasurably small. This effect is clearly illustrated in

38

Fig. 5.4, as the spacing between elements is decreased, the gradient approaches zero.

A small gradient implies that the output response will be difficult to measure due to a very small output voltage variation. This in turn would cause inaccuracies to creep in. In particular, it must be noted that the proportional region γ_p is based on an error term (Eq. 5.6), and thus measurements using a small gradient would not be accurate if the error term is large relative to the measurable output voltage.

5.5.2   Ambiguity of Response

Though a large spacing is unfavourable in terms of γ_p it becomes doubly unfavourable due to the ambiguity of received signal. The radiation pattern of two element array begins to repeat itself, with an increase of sidelobes. The effect of repeating signals is most apparent at spacings larger than 1λ as was seen in Fig. 4.5. Thus element spacings above 1λ will not be considered.

5.5.3   Input Impedance

The input impedance of each element may be considered to be the most important factor impacting on the optimisation of the system. Fig. B.1[7] illustrates the variation of feedpoint impedance with spacing. In general, this graph indicates that the smaller the element spacing the higher the feedpoint resistance. The graph requires that each element is parallel, self-resonant and operated in phase [1], factors that have been satisfied by the simplifying assumptions in this chapter. Also, it must be noted that for a smaller feedpoint resistance more current will flow for the same power applied [1], therefore radiating more energy. Looking at the graph it is apparent that a reasonable region of feedpoint resistance is say less than 70Ω. This would imply a spacing range of approximately 0.4λ to 0.95λ. This deduction would reduce the maximum possible range of γ_p to 37.2°.

---

[7] This figure is found in Appendix B as Figure: B.1.

Another important factor is that of mutual impedance. The relationship between mutual impedance and spacing is shown in Fig. B.2[8]. The region deduced above for favourable feedpoint impedance, namely 0.4λ to 0.95λ seems to be a reasonable region in terms of mutual impedance. Mutual impedance values become more favourable as the spacing increases. But, conversely these values become unfavourable below an element spacing of 0.4λ due to their large variations.

5.5.4 The Optimum Monopulse System

Table 5.2 below describes the optimal system in terms of angular range, spacing and gradient of response.

Table 5.2: The Optimum Monopulse System

Spacing s_1 (m)	Angular Range γ_p (°)	Gradient of Response
0.4λ	37.2	1.2
0.5λ	30.0	1.6

The optimal system setup related to $s_1 = 0.4\lambda$, has been determined taking into account the factors discussed earlier; input impedance, gradient of response and ambiguity. The spacing 0.5λ is also shown in Table 5.2 to compare discrepancies. Note an angular range discrepancy of $7.2°$ and greater gradient of response of 0.4 when a spacing 0.5λ is used. These are not large differences and thus it may be preferable to use the spacing of 0.5λ as the pattern is well-known and understood.

5.6 Conclusion

Using monopulse sensing techniques for angle measurement was determined to be a successful method for tracking a target over a specified angular range γ.

Firstly, a favourable spacing range between elements of $s_1 = 0.4\lambda$ to 0.95λ was found by investigating the effects of factors such as gradient response, ambiguity, feedpoint impedance and mutual impedance due to a change of spacing.

---

[8] This figure is found in Appendix B as Figure B.2.

Secondly, given this range and a further finding that a smaller element spacing would provide a greater angular range for tracking of a target, an element spacing of 0.5λ would be a reasonable choice. 0.5λ was chosen over 0.4λ as it's pattern is well known and understood. An element spacing of 0.5λ will be regarded as the optimum element spacing for the optimum monopulse system, which will find further applications in later chapters.

Further work could be performed in the region of investigating the effect of additional phase delay and lead in the feed of the antenna elements.

Chapter 6

Three Element Dipole Array

The purpose of this chapter is to investigate ways of steering a null in a particular direction with the aid of a third antenna element. The chapter will begin with a description of the antenna and receiver system arrangement. Various important properties of the three element array will also be stated and the electric field relationship between all points of interest will then be discussed. The formation of nulls due to a variation of spacing between the second and third element will be compared with the formation of nulls due to an added phase delay of the third element. Thereafter, a means to determine parameters that may accomplish cancellation of an interference signal received from a particular direction will be investigated. Finally, conclusions will be drawn.

6.1   Antenna and Receiver System Arrangement

Here the antenna and system structure will be introduced and important parameters thereof will be discussed. The figure below illustrates the antenna arrangement within the azimuthal plane.
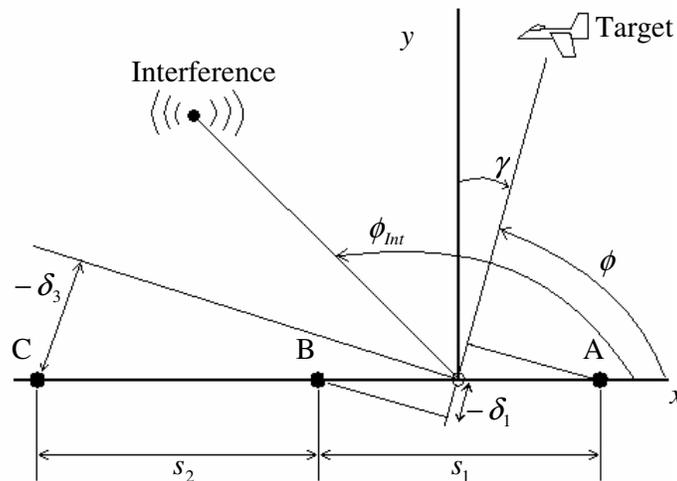

Figure 6.1: Arrangement of the antenna elements within the azimuth

The receiver system, involved in signal analysis, is shown in Fig 6.2.
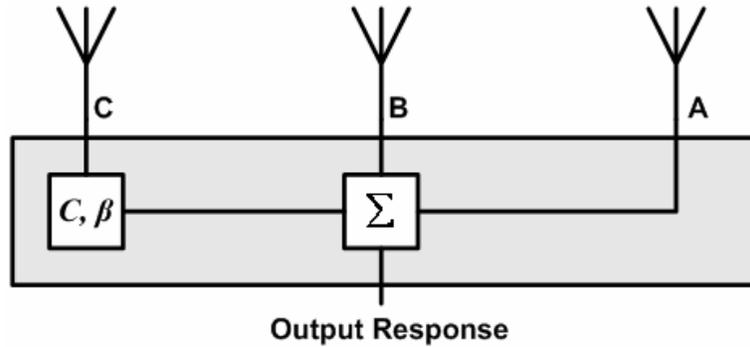
Figure 6.2: The receiver system represented here as a black box.

With the figures above as a reference the usual and some new simplifying assumptions are made. Planar waves can once again be assumed as both the point of interference and the target of interest lie within the far-field region. The target is assumed to be traveling on a trajectory a constant distance r from the phase center of the three element array. The interference signal is similarly also placed at a constant distance r from the phase center.

The variables used in Fig 6.1 will have the same properties as described in Chapter 4 and 5. A new addition in this chapter is the third antenna element denoted as element C and will also be a half-wave dipole element. It is assumed that the same current flows at the feed of element C as at the feeds of element A and B. This implies that the amplitude and magnitude of the electric fields $\hat{E}_1$, $\hat{E}_2$ and $\hat{E}_3$ at the elements A, B and C respectively are the same.

Another new addition is the point of interference. This point will be confined to an azimuth range of $\phi_{Int} \in [0°, 180°]$. It's angular position is measured from the x axis. This is different to the target, whose position is measured from the y axis. Though some analysis will be done over the entire azimuth range, this chapter will ultimately be concerned with the $\phi \in [0°, 180°]$ range. The target of interest seen in Fig 6.1 is not an important part of the analysis of this chapter, but is added for completeness. The subject of concern in this chapter will lie with the effect the point of interference has on the antenna array and how this effect can be minimised.

Fig. 6.2 shows the basic receiver system which will be concerned with manipulating signals received by the three antenna elements. In this chapter the manipulation will simply entail a variation of spacing s_2, phase delay β and gain C of the third antenna element. Its purpose is to achieve nulls in the direction of the point of interference. After the manipulation has been completed, the signals are summed and the resulting radiation pattern is investigated.

6.2　The Electric Field Relationships

Some important equations must be presented at this stage. These equations describe the relationship between the electric fields at the elements, the point of interference and the target. The core equation to the investigation in this chapter is:

$$\hat{E}_{sum} = \hat{E}_1(e^{j\delta_1} + e^{j\delta_2}) + \hat{E}_2(e^{-j\delta_1} + e^{-j\delta_2}) + C\hat{E}_3 e^{j\beta}(e^{-j\delta_3} + e^{-j\delta_4}) \ V/m \qquad (6.1)$$

Eq. 6.1 describes the output response shown in Fig. 6.2 and is based on derivation of Eq. 4.1. The total electric field at each element is given by:

$$\hat{E}_{element\ A} = \hat{E}_1(e^{j\delta_1} + e^{j\delta_2}) \ V/m \qquad\qquad (6.2)$$

$$\hat{E}_{element\ B} = \hat{E}_2(e^{-j\delta_1} + e^{-j\delta_2}) \ V/m \qquad\qquad (6.3)$$

$$\hat{E}_{element\ C} = C\hat{E}_3 e^{j\beta}(e^{-j\delta_3} + e^{-j\delta_4}) \ V/m \qquad\qquad (6.4)$$

where $\hat{E}_1$, $\hat{E}_2$ and $\hat{E}_3$ are calculated using Eq. 3.2 and the phase delays due to spacing are giving by:

$$\delta_1 = k(s_1/2)\cos\phi_{Tar} = k(s_1/2)\sin\gamma \ \ rad \qquad\qquad (6.5)$$

$$\delta_2 = k(s_1/2)\cos\phi_{Int} \ rad \qquad\qquad (6.6)$$

$$\delta_3 = k(s_2 + (s_1/2))\cos\phi_{Tar} = k(s_2 + (s_1/2))\sin\gamma \ rad \qquad\qquad (6.7)$$

$$\delta_4 = k(s_2 + (s_1/2))\cos\phi_{Int} \ rad \qquad\qquad (6.8)$$

The variables δ_1 and δ_3 of Eqs. 6.5 and 6.7 are shown in Fig. 6.1. δ_2 and δ_4 of Eqs. 6.6 and 6.7 are not shown as this would clutter the diagram, but they can be derived in the same way as δ_1 and δ_3. Using all these equations as a base, null forming was investigated.

6.3   Null Forming Analysis by Inspection

In this section the formation of nulls due to a variation of spacing s_2 and additional phase delay β will be investigated, by analysing and discussing different graphical representations.

6.3.1   Computation using Matlab

The analysis to follow was made possible by three Matlab scripts[9], namely ThreeVarySpacing.m, ThreeVaryPhase.m and FuncThreeElements_1.m. The algorithms within these scripts are based on the equations discussed above.

The script ThreeVarySpacing.m incrementally varies the spacing between the second and third element. At each increment of spacing s_2, the function FuncThreeElements_1.m is called. This function calculates the electric field in the far-field region over the entire azimuth range. Once the loop is complete ThreeVarySpacing.m determines the radiation pattern and plots it in the form of a surface. The surface is plotted relative to the entire azimuth range and the change of element spacing s_2.

In the same way ThreeVaryPhase.m calculates the change of the radiation pattern over a change in additional phase delay β in the third element as shown in Fig 6.2. FuncThreeElements_1.m is also called by this script to determine the electric field in the far-field region. As above, ThreeVaryPhase.m also illustrates the radiation pattern by plotting it in the form of a surface.

---

[9] See Appendix E.4 for a detailed description of the Matlab scripts of this chapter

6.3.2   *Analysis and Observations*

To begin with, ThreeVarySpacing.m is executed with the input parameters specified in Table 6.1.

Table 6.1: Input Parameters to ThreeVarySpacing.m

Input Parameters	Value
Minimum Spacing (λm)	0
Maximum Spacing (λm)	2.5
Additional Phase Delay β (rad)	0

The result is a radiation plot shown below:
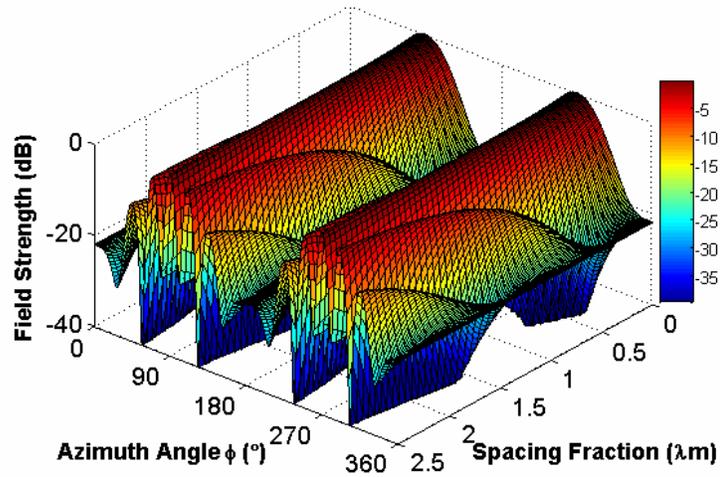
Figure 6.3: Radiation pattern due to variation of element spacing s_2.

It is important to note here that the variable s_2 is equal to a spacing fraction multiplied by λ. At an element spacing $s_2 = 0$ the deepest null is approximately 20dB. The major lobes are located at 90° and 270° in the azimuth. As the spacing s_2 is increased the most prominent feature of the plot in Fig 6.3 can be seen to be a rapid increase of the number of sidelobes and a subsequent decrease of the beamwidth of the two major lobes. This is not a desirable effect as an incoming signal becomes ambiguous and cannot be properly tracked due to the numerous partial nulls (approximately 20dB deep) between the sidelobes.

Next, ThreeVaryPhase.m is considered. The input parameters are given in table below.

Table 6.2: Input Parameters of ThreeVaryPhase.m

Input Parameters	Value
Minimum phase delay β (rad)	0
Maximum phase delay β (rad)	2π
Spacing s_2 (m)	0.5λ

Running the script ThreeVaryPhase.m the following radiation pattern is produced.
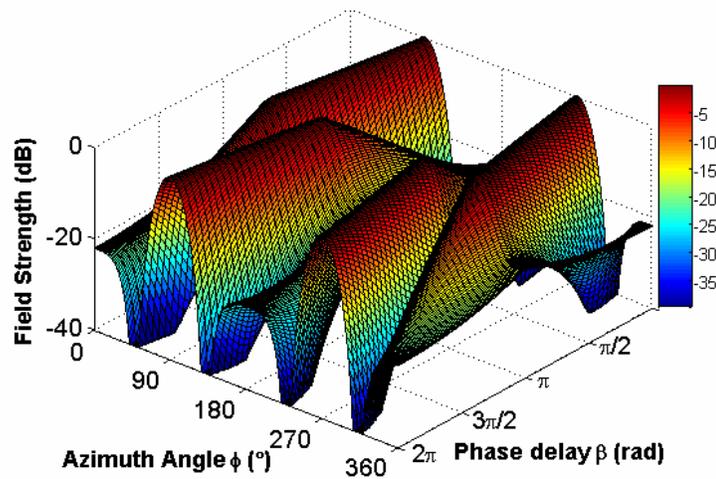
Figure 6.4: Radiation pattern to a change in the phase delay *β* of the third element.

At phase delay *β* = 0 rad the major lobes are at azimuth angles of 90° and 270°, with the deepest nulls found on either side of these major lobes. As *β* is increased to π rad the major lobes begin to skew towards a azimuth direction of 0° (360°) while at the same time two new lobes appear in the opposite direction, symmetrical about azimuth angle 180°. At π rad there are four relatively large lobes in the pattern. A further increase *β* sees a decrease in magnitude of the two original major lobes and a skewing of the two new lobes towards the 90° and 270° directions, putting the pattern back in its original state. This process would be repeated if *β* were increased above 2π rad.

To view any particular combination of phase delay *β* and spacing *s₂* as described above in a 2-D plot, the script ThreeElements.m can be used.

6.3.3 Conclusion

With reference to the diagrams above the following conclusion are drawn. Large values of spacing s_2 would be very unfavourable due to a rapid increase of sidelobes. Futhermore, the increase of sidelobes decreases the beamwidth of the major lobes, which is also undesirable in terms of target tracking. The radiation pattern produced by varying the phase delay β while keeping the s_2 constant did not show the serious degradation effects that an increase of spacing s_2 did. In particular, Fig 6.2 did not show any increase of sidelobes over its entire range.

For this reason, it can be concluded that when attempting null formation, a variation of phase delay will be preferred over a variation of spacing s_2.

In addition, there is a practical advantage of relying solely on phase (and gain) variation, namely one would not need to physically move any antenna hardware as variation of phase (and gain) can be done electronically.

Finally, due to the fact that a large spacing of s_2 has undesirable effects, it will be set to 0.5λ. Furthermore, from here on null formation will be investigated by varying only the phase and gain of element C as shown in Fig. 6.2.

6.4 Optimum Parameter Calculation

The focus of this investigation is to determine the parameters of phase delay β and gain C in order to create a pattern that forms a null in a particular direction. The element spacing s_2 will be kept constant at $\lambda/2$ due to the undesirable effects of its sidelobe build up at large spacings as found in the section above.

6.4.1 Computation of Parameters

The parameters of phase delay β and gain C are calculated by a Matlab script called ParameterCalc.m. Once these two parameters have been found, the script calls the function FuncThreeElements_2.m. FuncThreeElements_2.m must not be confused with FuncThreeElements_1.m of the above section. These functions have different input arguments. FuncThreeElements_2.m is a function that

calculates the radiation pattern of the antenna array for the calculated parameters phase β and gain C. The depth of the null and maximum response at 90° to the array axis (positive x axis) is also calculated in FuncThreeElements_2.m.

The Eq. 6.1 is modified as follows so as to determine the minimum possible response for an angle at which the point of interference is expected. The interference signals induced in elements A and B are of major interest. It is preferable that these are made as small as possible. To achieve this, the gain and phase delay must be chosen accordingly.

To this end Eq. 6.1 was reduced to:

$$\hat{E}_{TotInt} = \hat{E}_1(e^{j\delta_2}) + \hat{E}_2(e^{-j\delta_2}) + C\hat{E}_3 e^{j\beta}(e^{-j\delta_4}) \quad V/m \qquad (6.9)$$

which represents a summation of all the interfering signals in all the elements. ParameterCalc.m calculates $\hat{E}_{TotInt}$ for a variation of gain C and phase β for a point of interference at a specific angle ϕ_{Int}. It then proceeds by finding the minimum magnitude of $\hat{E}_{TotInt}$ and the associated C and β parameter values. As stated earlier, these values are then fed into FuncThreeElements_2.m providing the output radiation plot which illustrates that any signal coming from the specified interference position would be nulled.

6.4.2   *Analysis of Radiation Patterns*

Running the script files for variety of interference positions allows a number of interesting observations to be made. Spacings s_1 and s_2 as described in Fig 6.1 will remain constant at $\lambda/2$ throughout this investigation.

To begin with, two radiation patterns will be generated to illustrate null formation at particular positions.
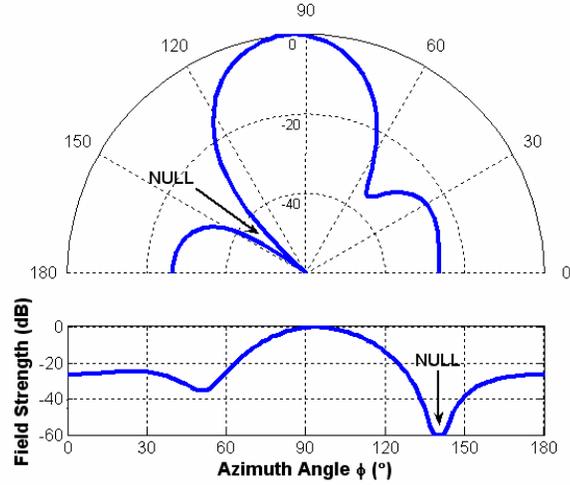
Figure 6.5: Radiation patterns with the interference point specified $\phi_{Int} = 140°$

The above figure illustrates a radiation pattern that was generated by simply inputting the angle of interference. The angle of interference is measured from the *x* axis. The information relevant to the above figure and found by running the script ParameterCalc.m is listed in Table 6.4.

Table 6.3: Properties related to Fig. 6.5 found by ParameterCalc.m

	Value
Interference Angle Φ_{int} (°)	140
Gain *C*	0.72
Phase Delay β (rad)	5.81
Null Depth (dB)	-98.66
Max Response at 90° (dB)	-0.09

The null depth at 140° seems to be very reasonable, and maximum response at 90° to the *x* axis is also only 0.09 dB below the normalized maximum. Thus using the parameters of *C* and *β* to manipulate the signal in the third element would result in a system that effectively reduces interference from an angle of $\phi_{Int} = 140°$ but yet still has a good response for signals arriving from the broadside direction, at $\phi = 90°$ from the *x* axis.

As a counter example, the point of interference will be placed at $\phi_{Int} = 90°$. Subsequently, running the ParameterCalc.m script results in a radiation pattern as illustrated below in Fig 6.6.
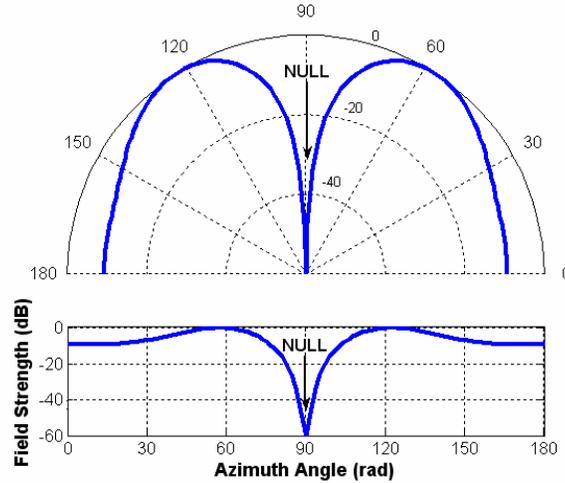

Figure 6.6: The radiation pattern with the interference point specified $\phi_{Int} = 90°$

Again the information related to Fig. 6.6 is provided in Table 6.5.

Table 6.4: Properties relative to Fig. 6.6 found by ParameterCalc.m

	Value
Interference Angle Φ_{int} (°)	90
Gain C	2
Phase Delay β (rad)	3.14
Null Depth (dB)	-47.52
Max Response at 90° (dB)	-47.52

With the interference point placed at $\phi_{Int} = 90°$, the null is still quite deep, though not as deep as at $140°$. Nevertheless, a wanted signal at this position would be cancelled along with the interference arriving from the broadside direction. This particular example of null formation merely indicates that a null can be formed in any direction by varying the phase delay and gain of the signal within element C.

The relationship between the maximum response at 90° and the variation of interference angle ϕ_{Int} can by investigated by looping the ParameterCalc.m for a

51

range of interference angles. This is done by a slightly modified script called ParameterCalcLoop.m. This relationship can be seen in Fig .6.7.
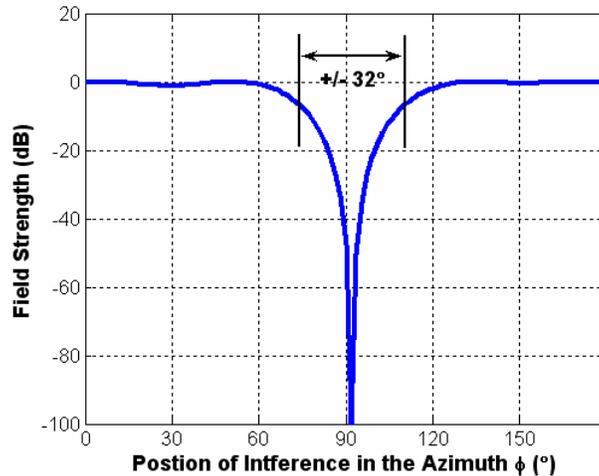

Figure 6.7: Relationship between Max Response at 90° and Interference Angle ϕ_{Int}

This graph presents an interesting relationship in the sense that the response in the broadside direction or at 90° counterclockwise from the *x* axis is at maximum for a very wide range of interference. For instance, if -6dB is considered an unacceptable drop in response gain, it is found that the range $\phi \in [74°, 106°]$ is the only unfavourable range as shown on the graph. And conversely, the response gain in the broadside direction is relatively large (above -6dB) for all interference positions outside the range $\phi \in [74°, 106°]$.

An assumption is now made that the interference signal will not pass over the region used for angle sensing as described in Chapter 5. This implies that nulls can freely and effectively be place in the range outside $\phi \in [74°, 106°]$ without having any undesirable effects on the reception of the target signal.

6.4.3   Conclusion

The results show that a sufficient null depth can be achieved with correct phasing and gain variation for any interference angle ϕ_{Int}. Furthermore, with the assumption that the interference signal will never arrive from the angular range allocated for angle sensing, the response from that range can be expected to be very high, namely above -6dB of the normalized field strength.

Chapter 7

Phase Monopulse Sensing with added Interference

The purpose of this chapter is to investigate ways in which monopulse angle sensing can be achieved with the presence of an interfering signal. The third element, introduced in Chapter 6, will be used to attempt a cancellation of the interference within the first and second antenna elements by means of changing the phase delay and gain of the incoming signal in element C. The chapter will begin with a description of the receiving system used. Monopulse angle sensing techniques will then be applied to the first two elements as was done in Chapter 5, starting with a situation where no attempt to cancel the interference is made. Thereafter, partial interference canceling will be dealt with and then finally full interference canceling will be investigated. Matlab was used as a tool whereby results were computed.

7.1   Receiver System Arrangement

The properties introduced and discussed in Chapter 6 regarding antenna arrangement, particularly Fig 6.1, are also applicable here. In this chapter more emphasis will be placed on the angle γ, the angle to the target of interest from the reference axis y. A significant change in this chapter from the last will be in terms of the receiver system. The black box will now manipulate signals as indicated in Fig 7.1.
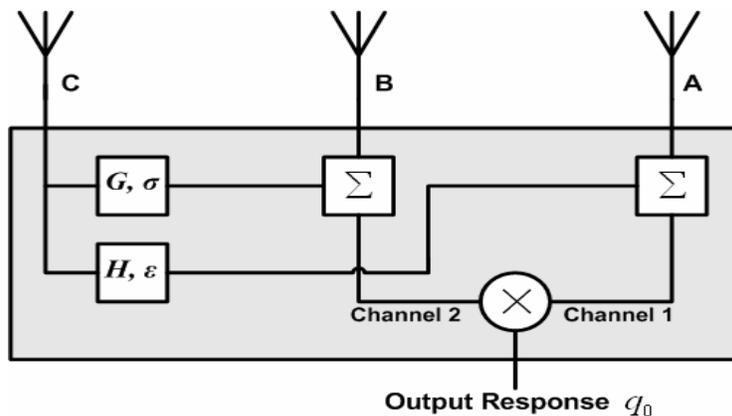

Figure 7.1: Receiver system used to manipulate signals

The investigation to follow in this chapter will all begin with the spacings s_1 and s_2 fixed at 0.5λ. The only factors to be varied will be the gain parameters *G, H* and phase delays σ, ε shown in Fig. 7.1. The idea here is that the interference received in elements A and B will be cancelled out before monopulse angle sensing is applied. The process of monopulse angle sensing makes use of the multiplicative angle sensing ratio and is shown in the Fig 7.1 as the multiplication sign between the two incoming channels.

7.2   Investigation of Signals Received

The Eqs. 6.1 through 6.8 also apply to the antenna and receiver system described above. Looking at Fig 7.1 it is noted that in order to achieve a situation where the signals after the summation points are free of interference, the signal from element C must be added in such a way so as to minimize the interference received in elements A and B. In terms of signal manipulation two equations will form the basis of the investigations to following this chapter. These equations were derived from Eqs. 6.1 through 6.8.

$$\hat{E}_{1\ CLEAN} = \hat{E}_{1Tar}e^{j\delta_1} + \hat{E}_{1Int}e^{j\delta_2} + H\hat{E}_3e^{j\varepsilon}(e^{-j\delta_3} + e^{-j\delta_4}) \quad V/m \qquad (7.1)$$

$$\hat{E}_{2\ CLEAN} = \hat{E}_{2Tar}e^{-j\delta_1} + \hat{E}_{2Int}e^{-j\delta_2} + G\hat{E}_3e^{j\sigma}(e^{-j\delta_3} + e^{-j\delta_4}) \quad V/m \qquad (7.2)$$

Where $\hat{E}_{1\ CLEAN}$ and $\hat{E}_{2\ CLEAN}$ represent the signals after the summation in the respective channels. *G, H* are gain values and σ, ε are phase delays as described in Fig. 7.1. The remaining variables of the above equations are discussed in Chapter 6.

7.3   Computation of Interference Cancellation

The first of the three investigations to be performed in this chapter will investigate monopulse angle sensing under the condition that no interference canceling will be done. This implies that the gain values of *H* and *G* in either channel will be set to zero thus canceling any effect of the third element. The Matlab script written to investigate this is called NoIntCancel.m.

The second investigation is performed by PartialIntCancel.m. This script calculates the minimum possible interference components in either channel such that the last two terms on the right of Eqs. 7.1 and 7.2 are at a minimum.

The third investigation assumes that element C is a directive antenna. This implies that the term related to $e^{-j\delta_3}$ (found in the brackets on the right side of Eqs. 7.1 and 7.2) within the third element can be assumed zero. This term describes the phase delay induced in element C by the target signal. In theory this method should give an even better response than that of the PartialIntCancel.m.

All these m.files[10] call the function CH7_PhaseMonopulse.m to perform the phase monopulse calculation.

Running each of the three scripts provides a graphical representation of the response similar to the one in Chapter 5. This allows comparisons to be made between the two. These graphical representations will once again form the basis of the analysis. Furthermore, the analysis will be done progressively beginning with NoIntCancel.m, which is followed with PartialIntCancel.m and finally ending with FullIntCancel.m.

7.4   No Interference Cancellation

This section investigates the implications of performing angle sensing monopulse on the two signals in channels 1 and 2 where no interference cancellation has been done.

7.4.1   *Computation and Analysis*

As mentioned, if no interference cancellation is attempted, *G* and *H* will be set to zero. This has the effect that monopulse sensing will be done on the signals in channel 1 and 2 that contain the complete signal components from both the target and interference. Eqs 7.3 and 7.4 below are derived from Eqs. 7.1 and 7.2.

$$\hat{E}_{1\ CLEAN} = \hat{E}_{1Tar}e^{j\delta_1} + \hat{E}_{1Int}e^{j\delta_2} \quad V/m \tag{7.3}$$

---

[10] See Appendix E.5 for a detailed description of the Matlab script relevant to this chapter

$$\hat{E}_{2\ CLEAN} = \hat{E}_{2Tar}e^{-j\delta_1} + \hat{E}_{2Int}e^{-j\delta_2} \quad V/m \tag{7.4}$$

Applying phase monopulse sensing techniques to these to signals results in the following relationship illustrated in Fig. 7.2.
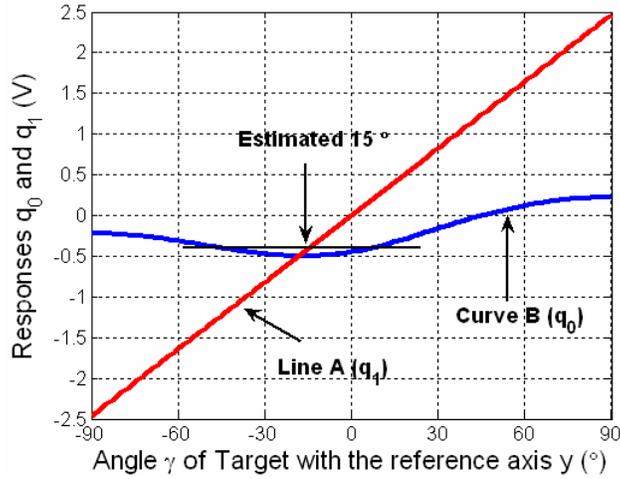

Figure 7.2: Responses q_0 and q_1 relative to the angle γ of the target, under the condition of no interference cancellation

From this figure it can clearly be seen that a large error in angle reading will occur. Firstly, there is no proportional region. Secondly, there is an offset from the origin in the order of -0.4V. Thus, broadside to the antenna array or if γ were equal to 0° then the output of the system would give -0.4V. Using this voltage and the linear approximation shown by line A as a reference, the target will be estimated at an angle 15° counterclockwise from the reference axis. This error would be unacceptable.

7.4.2 Conclusion

All in all, if the interference is not canceled in each channel no phase monopulse sensing can be done. In order for this system to work the real response q_0 must pass through the origin and there must also be a reasonable range over which the response is proportional to the linear approximation q_1. But as can be seen this is not the case and thus another approach must be investigated.

7.5   Partial Interference Cancellation

For a variation of target position the parameters *G, H* and σ, ε of Eqs. 7.1 and 7.2 are calculated with the objective of minimizing the interference components in channels 1 and 2 so that monopulse angle sensing can be performed with better results than as found above.

7.5.1   *Computation and Analysis*

Varying the target's position in the azimuth for $\gamma \in [-90°, 90°]$ the parameter values were calculated using a reduced version of Eqs. 7.1 and 7.2, namely:

$$\hat{E}_{C1\ INT} = \hat{E}_{1Int}e^{j\delta_2} + H\hat{E}_3 e^{j\varepsilon}(e^{-j\delta_3} + e^{-j\delta_4})\ \ V/m \tag{7.5}$$

$$\hat{E}_{C2\ INT} = \hat{E}_{2Int}e^{-j\delta_2} + G\hat{E}_3 e^{j\sigma}(e^{-j\delta_3} + e^{-j\delta_4})\ \ V/m \tag{7.6}$$

$\hat{E}_{C1\ INT}$ and $\hat{E}_{C2\ INT}$ above represent the total interference components in channels 1 and 2 respectively. For each position of the target in the range of γ a range of gain values (*G* and *H*) and a range of phase delays (σ and ε) forming a matrix were tested to find the minimum possible magnitudes for $\hat{E}_{C1\ INT}$ and $\hat{E}_{C2\ INT}$. Table 7.1 represents these and other important input parameters specific to the Matlab script PartialIntCancel.m.

Table 7.1: Input Parameters of PartialIntCancel.m

	Value
Range of Target Position γ (°)	ϵ [-90°, 90°]
Range of Gain *G, H*	ϵ [0, 4]
Range of Phase Delay *σ, ε* (rad)	ϵ [0, 2π]
Interference Position Φ_{Int} (°)	135°
Spacings s_1 and s_2	λ/2

Refer to Fig 6.1 for a recap on the properties of spacings s_1 and s_2 and interference position Φ_{Int}.

Running PartialIntCancel.m with the values specified in Table 7.1, results in the following. First off, the parameters *G, H,* σ and ε for the minimum possible

magnitudes for $\hat{E}_{C1\ INT}$ and $\hat{E}_{C2\ INT}$ (or maximum interference cancellation) are found and presented in the Fig. 7.3 and 7.4.
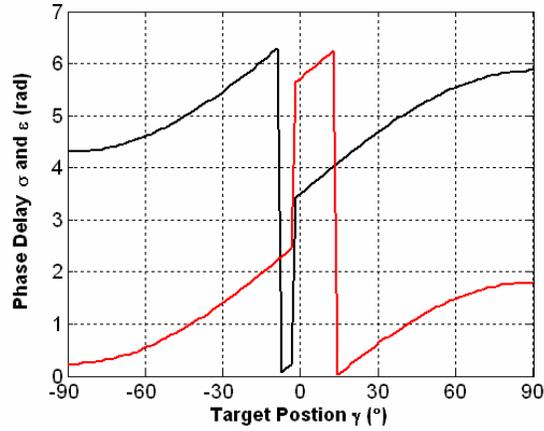

Figure 7.3: Phase delay values σ (red) and ε (black) for minimum possible interference over the target range γ.
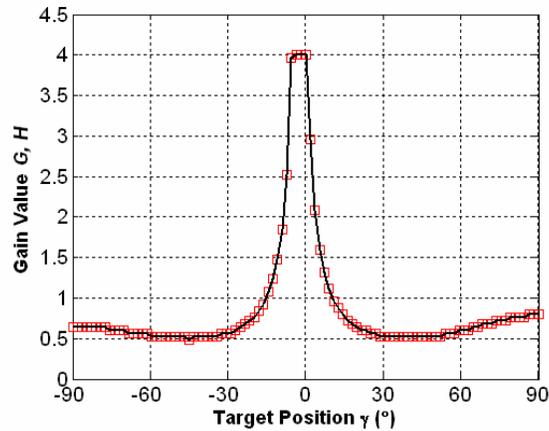

Figure 7.4: Gain values G (red) and H (black) for minimum possible interference over the target range γ.

Two things can be noted when considering Fig 7.3. Firstly, there is a constant phase difference between the values of the two phase delays as indicated on the figure. Secondly, at $\gamma = 0°$ there is a π rad jump in the phases as the target crosses the broadside position. This jump is due to the output response q_0 crossing the zero point.

In terms of gain, the Fig. 7.4 shows that the two values of G and H are equal for the entire range of target position. Also, as the target moves over, or looking more

closely at the figure just left of, the broadside position the gain saturates at its maximum specified value of 4.

Now, the implications of these two sets of parameter properties can be seen when the output response q_0 (from the multiplicative sensing ratio) is considered.
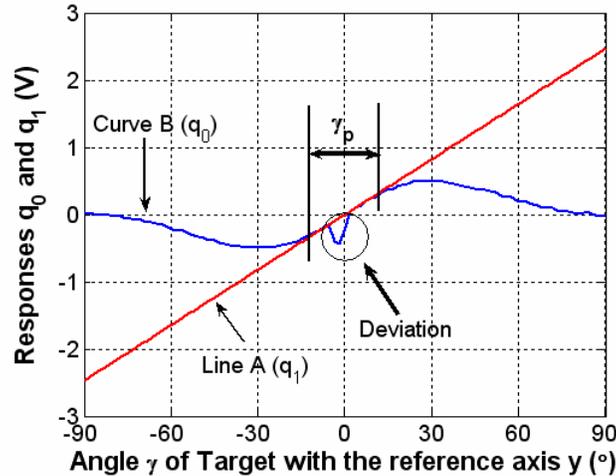

Figure 7.5: Responses q_0 and q_1 relative to the angle γ of the target, under the condition of partial interference cancellation ($s_2 = 0.5\lambda$).

A deviation, shown inside the circle, from what was found in Chapter 5, can clearly be seen in Fig. 7.5. This is a very unfavourable effect as it reduces the possible angle sensing range by the size of the deviation. In this case the angle sensing range γ_p is effectively halved to 16°, from its original value found in Chapter 5 and presented in Table 5.2.

The core cause of this deviation is due to the term $(e^{-j\delta_3} + e^{-j\delta_4})$ found both in Eqs. 7.5 and 7.6. A vector representation of the two factors within this term shows what is occurring at this point of interest, when the target passes by the broadside position. The vectors in the figure below illustrate the phase delays of the incoming interference and target signals induced within element C.
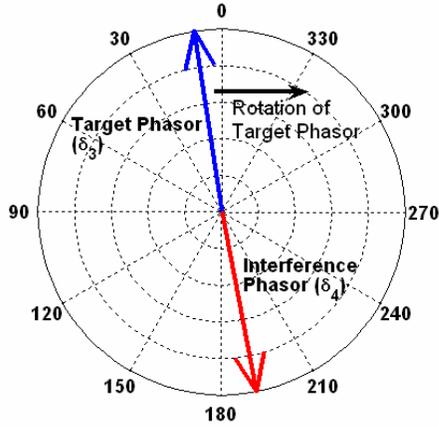
Figure 7.6: Vector representation of phase delays of the target (δ_3) and interference (δ_4) signals

The interference vector remains constant at the position indicated for the values specified in Table 7.1. As the target traverses its trajectory over the range $\gamma \in [-90°, 90°]$ its phasor passes directly opposite to the interference phasor as shown in Fig.7.6. This causes the term ($e^{-j\delta_3} + e^{-j\delta_4}$) to become infinitely small and in response to this the gains G and H increase as seen in Fig. 7.4. However, both gains are limited to a finite value of 4 and are unable to compensate for the deviation. The implications of this are such that second terms on the right hand side of Eqs. 7.5 and 7.6 tend to zero leaving the interference components of $\hat{E}_{1Int}e^{j\delta_2}$ and $\hat{E}_{2Int}e^{-j\delta_2}$ in channels 1 and 2 intact.

To counteract this degrading effect the spacing s_2 between elements B and C can be slightly varied. Keeping in mind the unfavourable effects of large spacings of s_2 found in Chapter 6, s_2 is now set to 0.9λ. Following the same procedure as before, the output response q_0 is found and shown in Fig. 7.7 below.

61
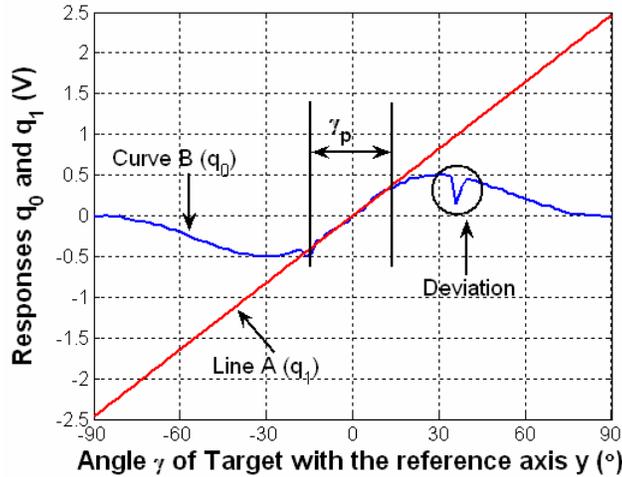
Figure 7.7: Responses q_0 and q_1 relative to the angle γ of the target, under the condition of partial interference cancellation ($s_2 = 0.9\lambda$).

Having changed s_2 to 0.9λ, the proportional range described by γ_p is seen to be free of any major degrading deviations. The degrading deviation has moved to the indicated position outside the proportional range γ_p, restoring γ_p to its original value of 30°.

Another observation that can be made by looking at Fig. 7.7 is that the response q_0 seems to be noisy inside the range γ_p. Despite this effect, the relationship presented in Fig. 7.7 still satisfies the *error* term described by Eq 5.6.

7.5.2   Conclusion

These findings presented a method of canceling interference in channels 1 and 2 for the purpose of monopulse angle measurement. This method proved successful, but required a variation of a number of parameters for accurate tracking of a target. This is not entirely favourable, as such a system would require significant signal analysis and control systems. Furthermore, undesirable noise seemed to be present in the output response, but was concluded to be inconsequential.

7.6 Full Interference Cancellation

The final investigation is based on the assumption that element C is a directive antenna element. This implies that the antenna can be positioned in such a way as to solely pick up the interfering signals.

7.6.1 Computation and Analysis

Applying the idea of directivity, the term ($e^{-j\delta_3}$) in Eqs. 7.5 and 7.6 is set to zero so as to get:

$$\hat{E}_{C1\ INT} = \hat{E}_{1Int}e^{j\delta_2} + H\hat{E}_3 e^{j\varepsilon}(e^{-j\delta_4})\ V/m \qquad (7.7)$$

$$\hat{E}_{C2\ INT} = \hat{E}_{2Int}e^{-j\delta_2} + G\hat{E}_3 e^{j\sigma}(e^{-j\delta_4})\ V/m \qquad (7.8)$$

The same procedures followed in the previous section will once again be followed here. The goal as before, is to find the parameter values of *G, H,* σ and ε so as obtain the minimum possible magnitudes of $\hat{E}_{C1\ INT}$ and $\hat{E}_{C2\ INT}$.

The same input parameters as stated in Table 7.1 will be used. Now, running the script FullIntCancel.m returns the following results in terms of *G, H,* σ and ε.


(a)   (b)
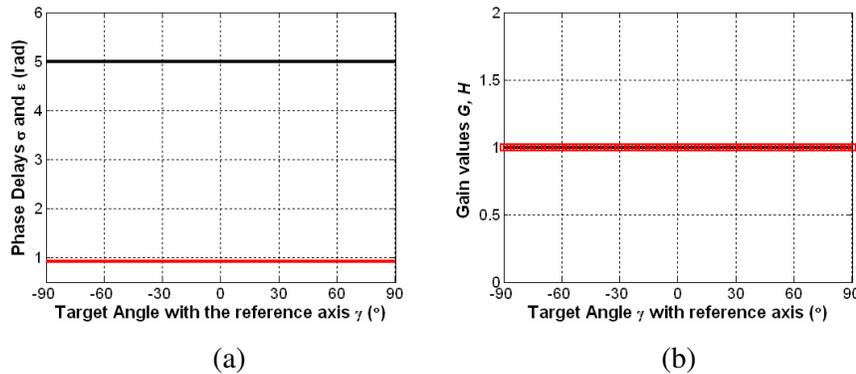
Figure 7.8: Parameter values of (a) phase delays (σ and ε) and (b) Gain (*G* and *H*) for minimum possible interference for FullIntCancel.m

Fig. 7.8 shows constant values for all parameter values. The parameters associated with channel 1 (H, ε) are given in black and the parameters associated with

63

channel 2 (G, σ) are given in red. G and H are equal and constant. Phase delays σ and ε are also constant but are phase shifted from one another by 4.08 rad (equivalent to 234°) as seen in Fig. 7.8(a). This is a significant change from the parameters found in the last section.

The reason for these constant values can be explained again in terms of vectors.
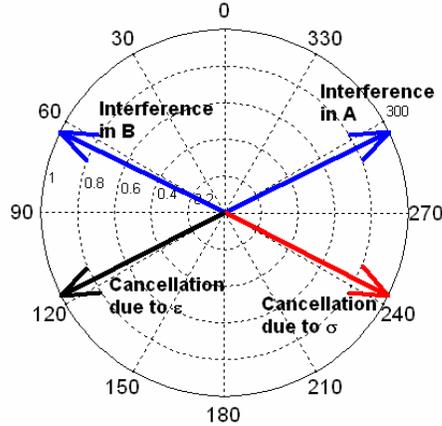

Figure 7.9: Vector representation of parameter phase delays and interference phase delays.

The vectors represented in Fig 7.9 are produced with the input parameters listed in Table 7.1. They are of constant magnitude and also have constant phase delays, meaning that as the target traverses its trajectory the vectors do not rotate. The major feature of interest here is the phase relationships. Firstly, interference in element A is induced with a lagging phase and interference in element B is induced with a leading phase. The parameters σ and ε are then calculated so as to form anti-phase relationship with the interference in elements A and B effectively reducing $\hat{E}_{C1\ INT}$ and $\hat{E}_{C2\ INT}$ to zero which in turn reduces Eqs. 7.3 and 7.4 to:

$$\hat{E}_{1\ CLEAN} = \hat{E}_{1Tar}e^{j\delta_1} \quad V/m \tag{7.9}$$

$$\hat{E}_{2\ CLEAN} = \hat{E}_{2Tar}e^{-j\delta_1} \quad V/m \tag{7.10}$$

64

To observe the implications of this behaviour, monopulse sensing is performed on the two signals $\hat{E}_{1\ CLEAN}$ and $\hat{E}_{2\ CLEAN}$ coming out of the summation blocks of Fig. 7.1. The result is seen in Fig 7.10.
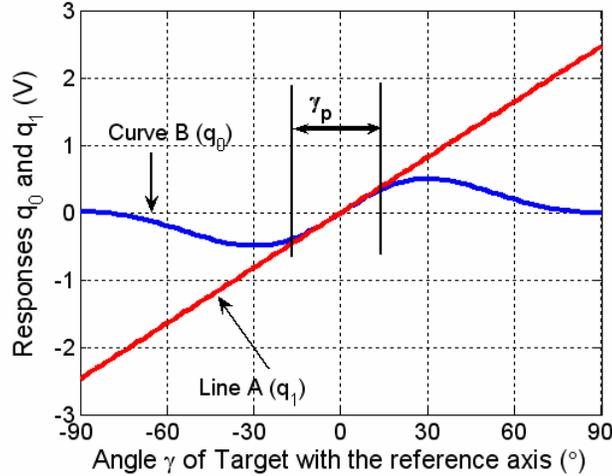

Figure 7.10: Response of q_0 and q_1 for a variation of target angle γ, under the condition of full interference cancellation

Fig. 7.10 shows a very clean response of q_0, much like the response found in Chapter 5. Calculating the angular range of γ_p over which the response q_0 is proportional finds $\gamma_p = 30.6°$. This relates very closely with the value found in Chapter 5 in Table 5.2 for an element spacing $s_1 = 0.5\lambda$.

7.6.2   Conclusion

The condition of full interference cancellation where the third antenna element is assumed directive was found to be very successful for angle measurement. This method does not present the unfavourable effects of deviations and noise that were found under the condition of partial interference cancellation. Consequently, this is the most desirable method when angle measurements are to be taken using phase monopulse techniques.

Chapter 8

Conclusions and Future Work

This thesis investigated the feasibility of a number of methods and techniques to achieve beam forming and null placement, with the ultimate goal of target tracking. The properties, favourable and unfavourable, of these methods and techniques were analysed and discussed in detail to determine optimum antenna system parameters.

The establishment of a firm literary base was believed important. Thus to this end, a great deal of literature was studied and reviewed and ultimately presented in Chapter 2 of this thesis.

The actual analytical work done in this thesis began by setting a foundation with an investigation into a single omnidirectional half-wave dipole element. The addition of a second identical antenna element showed the possibility of simple beam forming with a variation of phasing and spacing of the two elements. Though, at the same time it was found that a fixed null could not be placed in one particular direction while beam forming was taking place.

Using monopulse sensing techniques [4] for angle measurement was determined to be a successful and effective method for tracking a target over a specified angular range. This range is desired as large as possible but is constrained by factors of gradient response, ambiguity and input impedance. Subsequently, the optimum monopulse system for a two element array was determined to be at an element spacing of $0.5\,\lambda$.

The addition of a third antenna element to the array, provided a means of steering a null in any particular direction while keeping a reasonable response in the broadside direction. Furthermore, the addition of the third element enabled monopulse sensing techniques to successfully track a target signal despite the presence of an added interfering signal. In particular, the case of using a directive third antenna element for interference canceling in a monopulse system proved to be indeed the most desirable and optimal method investigated for target tracking in this thesis.

66

In terms of future work, much additional analytical work can be done to further the investigations begun in this thesis. In particular, the investigations done in Chapter 7 can be furthered by looking into possible applications to a practical system. This said, the work done in this thesis was purely of an analytical nature. Subsequently, all the investigations and analyses carried out here could be verified by practical implementation.

Appendix A: Derivations

A.1: Derivation 1

$$|\delta| = k\frac{s_1}{2}\cos\phi \ = k\frac{s_1}{2}\cos(\frac{\pi}{2} - \gamma) \ = k\frac{s_1}{2}\sin(\gamma)$$

The above equation is represented in the text as Eq. 5.2

A.2: Derivation 2

According to Peebles the one-way complex receiving voltage pattern is specified as [4]:

$$p(\gamma) = f(\gamma)e^{j\beta(\gamma)}.$$

See Chapter section 2.3.2 on pattern representation to see how this expression was derived. The multiplicative angle sensing ratio was defined as [4]:

$$r_m(\gamma) = \frac{p(\gamma)}{p(-\gamma)} = e^{2j\beta(\gamma)}.$$

Following the deduction of Peebles a complex voltage R is found to be [4]:

$$R = \frac{-jV_0^2}{2}r_m(\gamma).$$

Using the expressions above the real output q_0 of the complex response R above can be shown to be proportional to γ for small angles of γ [4]. I.e.:

$$q_0 = \text{Re}(R) = \frac{V_0^2}{2}\sin(\frac{2\pi s_1}{\lambda}\sin\gamma).$$

The above expression is represented in the text as Eq. 5.4.

Appendix B: Relationship Graphs
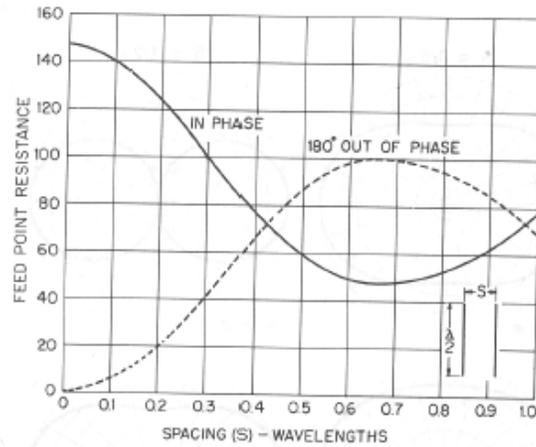
Figure B.1: Feed point resistance measured at the center of one element as a function of spacing between two parallel half-wave self-resonant antenna elements [1].
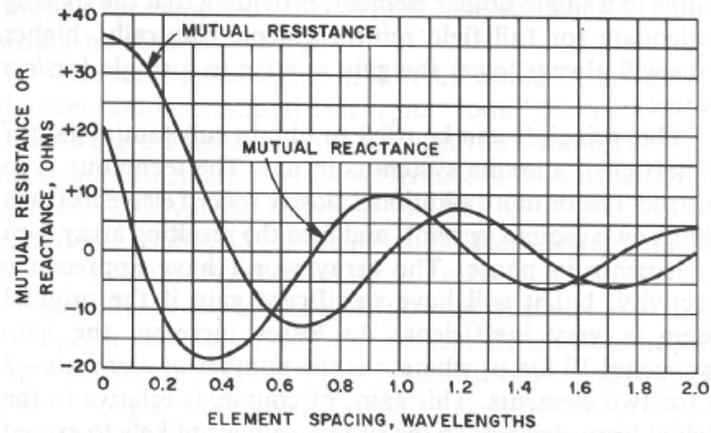
Figure B.2: Mutual impedance between two parallel quarter-wave vertical elements. Multiply the resistance and reactance values by two for half-wave dipoles [1].

Appendix C: The ARRL Radiation Patterns [1]
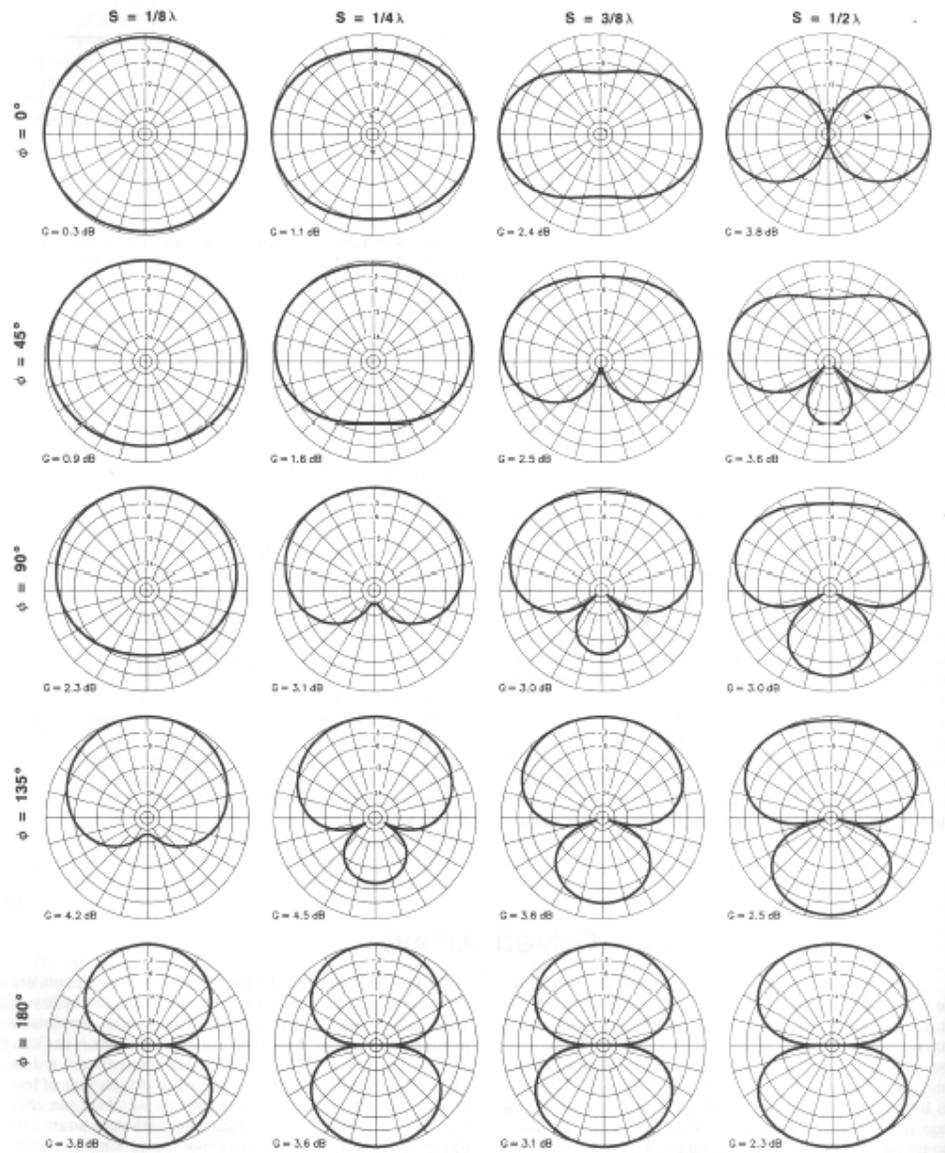
Figure C.1 (a)
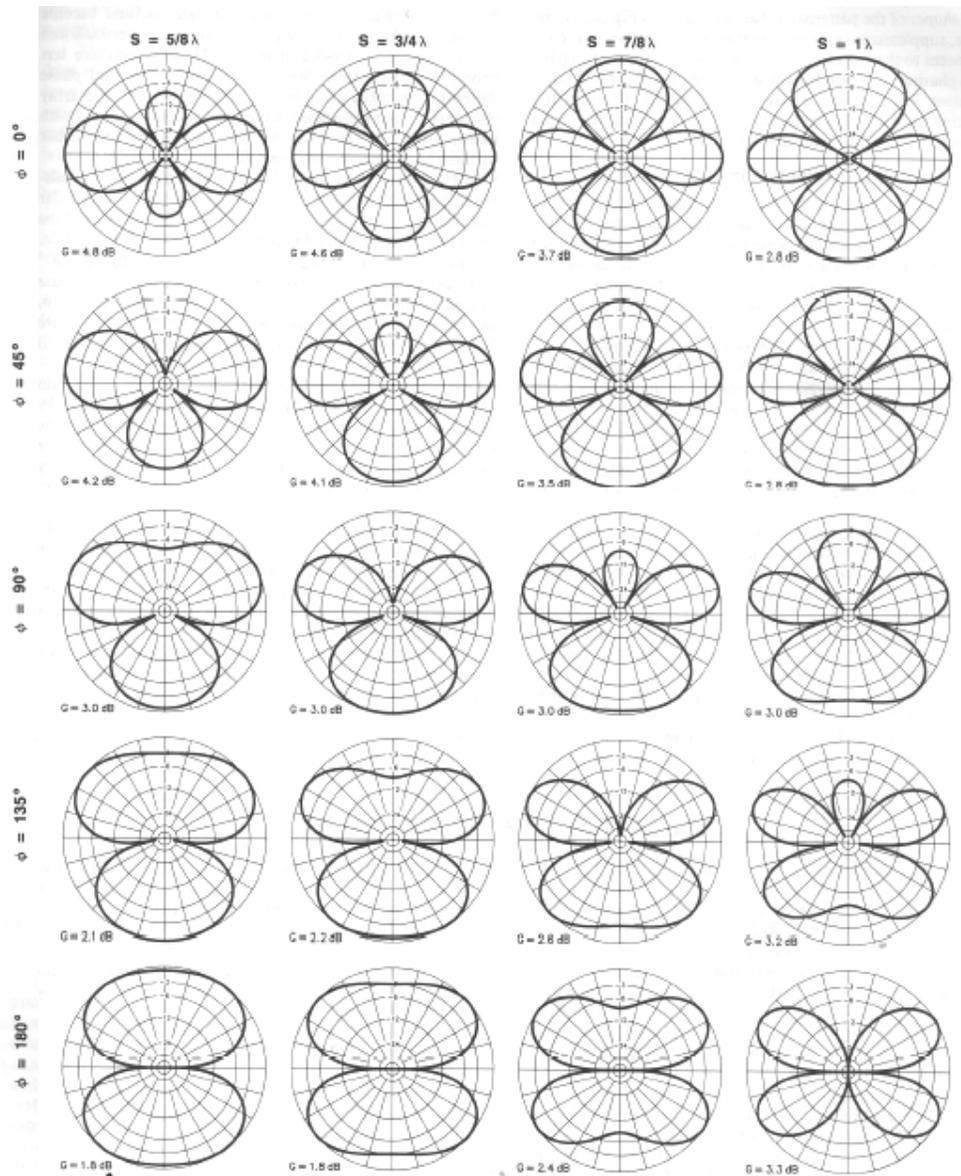
Figure C.1 (b)

Figure C.1: Azimuth (H-plane) patterns of two identical parallel driven elements, spaced and phased as indicated (S = spacing, ϕ = phasing). The elements are aligned with the vertical (0°, -180°) axis, and the element nearer the 0° direction (top of the page) is of lagging phase at angles other than 0°. The two elements are assumed to be thin and self-resonant, with equal-amplitude currents flowing at the feed point. The plots represent the free-space vertical or elevation pattern of two horizontal half-wave elements when viewed on end, with one element above the other [1].

Appendix D: Makarov Code Sequence Diagram [5]
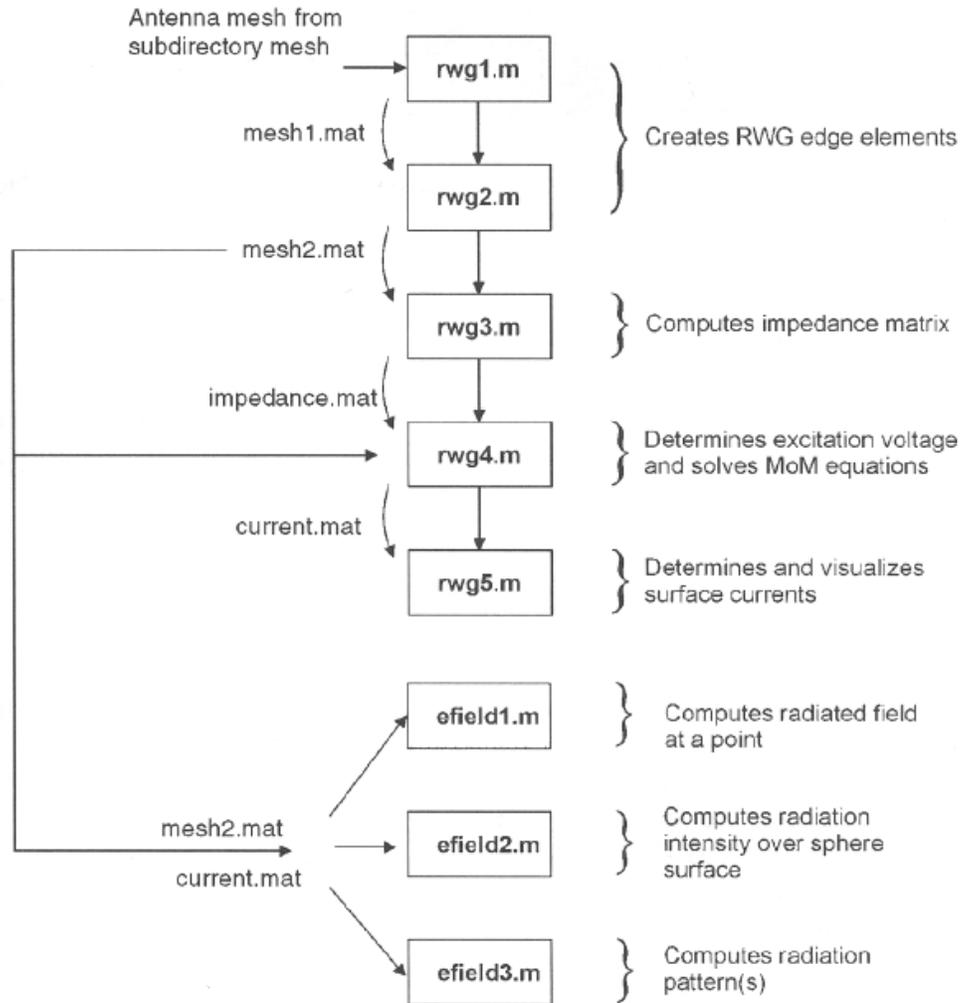
Figure D.1: Flowchart of the complete radiation algorithm [5]

# Appendix E: Matlab Code Description

The Matlab scripts written for this thesis are found on the CD provided. All the m.files presented in each chapter are located in separate folders. For instance, the Matlab scripts of used in Chapter 5 are found in a folder on the CD called Chapter5. This appendix lists all the m.files contained in each chapter folder and gives a brief description. The descriptions are also found in the actual scripts.

E.1 - Chapter 3 Single Half-Wave Antenna Element

The following Matlab scripts are found in the folder Chapter3 on the CD provided.

Relevant Scripts:

SingleElement.m

Description:

SingleElement.m:
This Matlab script is a stand alone script that calculates the amplitude radiation pattern.

E.2 - Chapter 4 Two Element Dipole Array

The following Matlab scripts are found in the folder Chapter4 on the CD provided.

List of Scripts

TwoElements.m
Ch4_GUI.m
SpecificValues.m
VarySpacing.m
VaryPhase.m
FuncTwoElements

Description

TwoElements:

This m.file builds on SingleElement.m. Here a second half-wave dipole element is added. The purpose of this m.file is to investigate the effects of a change of spacing and phasing between two elements on the radiation pattern. The calculation of the electric fields is based on 4.1 in the thesis.

ch4_GUI.m:

This m.file provides a graphical user interface to enable the user to input parameters of spacing and phasing easily and quickly. This GUI calls upon three other m.files, namely, VarySpacing.m, VaryPhase.m and SpecificValues.m. It provides the user with the option of producing a surface of a varying parameter or of producing a single plot with specific parameters.

SpecificValues.m:

This function is called by ch4_GUI. It itself calls the FuncTwoElements.m function and plots the calculated electric field of two elements in a polar and rectangular coordinate system.

VarySpacing.m:

This function is called by ch4_GUI.m. It calculates the electric field by calling the function FuncTwoElements.m. Finally, it illustrates the radiation pattern over the entire azimuthal range as a function of varying spacing at a constant specified feed phase.

VaryPhase.m:

This function is called by ch4_GUI.m. It calculates the electric field by calling the function FuncTwoElements.m. Finally, a surface is plotted that illustrates the radiation pattern over the entire azimuthal range as a function of varying feed phase in one of the two antenna elements at constant specified spacing between the two antenna elements.

FuncTwoElements.m:

This m.file is a function and is called by SpecificValues.m, VarySpacing.m and VaryPhase.m (these 3 are all functions), all of which are called by the ch4_GUI.m. FuncTwoElements.m calculates the electric field in the far-field region. This is done so as to plot various radiation patterns.

E.3 - Chapter 5 Angle Sensing Using Phase Monopulse

The following Matlab scripts are found in the folder Chapter5 on the CD provided.

List of Scripts

PhaseMonopulse.m
LoopPhaseMonopulse.m
FuncPhaseMonopulse.m

Description

PhaseMonopulse.m:

This m.file uses phase monopulse to determine the angle of arrival of a target and also the effective range over which a target can be accurately tracked. In particular the multiplicative angle sensing ratio was used [4].

LoopPhaseMonopulse.m:

The purpose of this m.file is to calculate the proportional range of the output response q_0. This proporitonal range describes the range over which the target's angle can accurately be sensed. The result is visualised with the aid of a graph of γ_p vs element spacing s_1.

FuncPhaseMonopulse.m:

This m.file is a function that is called by LoopPhaseMonopulse.m. The purpose of this function is to calculate the angular range over which the response q_0 is proportional.

E.4 - Chapter 6 Three Element Dipole Array

The following Matlab scripts are found in the folder Chapter6 on the CD provided.

List of Scripts

ThreeElements.m

ThreeElementsCheck.m

ThreeVarySpacing.m

ThreeVaryPhase.m

FuncThreeElements_1.m

ParameterCalc.m

ParameterCalcLoop.m

FuncThreeElements_2.m

Description:

ThreeElements.m:

This m.file builds on TwoElements.m. Here a third half-wave dipole element has been introduced. The purpose of this m.file was to investigate the effects of spacing and phasing of the third element on the radiation pattern.

ThreeElementsCheck.m:

This m.file was written to check the output of ThreeElements.m. It can only check ThreeElements.m for constant spacing between elements, and thus is only useful once off. The equation used in this script was found in the Antenna Design Handbook [9].

ThreeVarySpacing.m:

This m.file calls FuncThreeElements_1.m to calculate the electric field which it then illustrates over the entire azimuthal range as a function of varying spacing of the third dipole element (C). The first two antenna elements (A and B) have a constant element spacing.

ThreeVaryPhase.m:

This m.file calls FuncThreeElements_1.m to calculate the electric field which it then illustrates over the entire azimuthal range as a function of varying phasing of the third dipole element. It plots the logarthim of the voltage in the signal. The first two antenna elements have constant element spacing and are not shifted in phase by an additional phase shift.

FuncThreeElements_1.m:

This function is called by the m.files ThreeVarySpacing.m and ThreeVaryPhase.m. It calculates the electric field in the far-field produced by the three elements and returns it to the two aforementioned m.files.

ParameterCalc.m:

This m.file calculates the values of the phase delay and gain necessary for adjusting the signal in element C in order to cancel interference in a particular direction picked up by the entire array. It achieves this by checking a range of gain and phase delay values for the interference position concerned.

ParameterCalcLoop.m:

This m.file calculates the values of the phase delay and gain necessary for adjusting the signal in element C so that it cancels all interference in a particular direction. This script is different to ParameterCalc.m in that it varies the angular position of the interference signal over a range phiInt [0, pi].

FuncThreeElements_2.:

This function is called by the m.file ParameterCalc.m. Note that it is not the same as FuncThreeElements_1.m. This function also calculates the position of the null and the broadside position.

E.5 - Chapter 7 Phase Monopulse Sensing with added Interference

The following Matlab scripts are found in the folder Chapter7 on the CD provided.

List of scripts

Nointerference.m

NoIntCancel.m

PartialIntCancel.m

FullIntCancel.m

CH7_Monopulse.m

Description

NoInterference.m:

This m.file investigates the case where no interference is present. The properties found by this script should be very similar to the properties found in PhaseMonopulse.m of Chapter 5.

NoIntCancel.m:

This m.file investigates the situation where the element C is disregarded and phase monopulse sensing is done on the signals in elements A and B with the full effect of interference. To do the phase monopulse calculation the function CH7_Monopulse.m is called.

PartialIntCancel.m:

This m.file investigates the situation where both the interference and target signals are present in element C. An attempt to cancel the interference in elements A and B is carried out by varying the gain and phase delays for each channel. Monopulse sensing is carried out on the signals in channels 1 and 2 with the function CH7_PhaseMonopulse.m.

FullIntCancel.m:

This m.file presents the hypothetical situation where the third antenna element C is a directive antenna and is steered such that it only picks up the interference signal. Subsequently, gain and phase delay values are calculated in order to cancel out the interference in elements A and B so that monopulse sensing can be perform on the signals in channels 1 and 2. To this end the FullIntCancel.m script calls CH7_Monopulse.m.

CH7_PhaseMonopulse.m:

This m.file is a function that is called by the m.files PartialIntCancel.m, NoIntCancel.m, FullIntCancel.m and NoInterference.m. It performs phase monopulse on the signals of the first two elements A and B. It also calculates the gradient of the response according to Peebles [4].

Appendix F: CD

This thesis comes with a CD containing:

- All Matlab scripts discussed in this thesis.

- A PDF version of this thesis.

- A word doc of this thesis.

References

[1]   *The ARRL Antenna Book.* The American Radio Relay League, 1994.

[2]   David M. Pozar. *Microwave and RF Design of Wireless Systems.* John Wiley & Sons, 2001 (pg. 111 – 138).

[3]   Nicholas C. Currie. *Radar Reflectivity Measurement: Techniques & Applications. ARTECH House, 1989.*

[4]   Peyton Z. Peebles Jr. *Radar Principles.* John Wiley & Sons, 1998.

[5]   Sergey N. Makarov. *Antenna and EM Modeling with MATLAB$^{\circledR}$.* John Wiley & Sons, 2002.

[6]   Wikipedia. Wikipedia, the free encyclopedia – http://en.wikipedia.org/wiki/Passive_radar, September 2006

[7]   Wikipedia. Wikipedia, the free encyclopedia – http://en.wikipedia.org/wiki/Multistatic_radar, September 2006

[8]   G. R. Jessop. *VHF/UHF Manual, Fourth Edition.* Radio Society of Great Britain, 1983.

[9]   A.W. Rudge et al. *The Handbook of Antenna Design Volumes 1 and 2.* Peter Peregrinus Ltd, 1986.

[10]   ICASA. *Final Terrestrial Broadcast Frequency Plan 2004.*

[11]   P. Lorrain et al. *Electromagnetic Fields and Waves, Third Edition.* W. H. Freeman and Company, 1988.

[12]   Sentech. South African based Broadcaster. http://www.sentech.co.za , October
        2006